



School of Chemistry

Plasma-Assisted Growth of Single Crystal, Boron Doped Diamond Schottky Junctions

Fraser Crawford

**This thesis is submitted in partial fulfilment of the requirements for the Honours Degree
of MSci at the University of Bristol**

Prof. Neil Fox

Prof PW May

Bristol University Diamond Group

Abstract

In this work, a procedure for growing conductive boron-doped diamond layers on (110) orientated single crystal diamond using microwave plasma chemical vapour deposition (CVD) was found using a forward microwave power of 1.35kW, a pressure of 100 Torr, a temperature of 1090°C, a [CH₄]/[H₂] ratio of 1% and a [B₂H₆]/[CH₄] ratio of 667 ppm. These layers were examined with scanning electron microscopy to find a growth rate of 1.5 μm h⁻¹. A boron doped layer sample from this recipe along with another hot filament CVD grown sample was then topped with an unintentionally doped diamond intrinsic layer. These structures were then metallised with a nichrome/gold bilayer contact on the exposed boron doped layer and a aluminium/gold bilayer contact on the intrinsic layer. This formed a psuedo vertical Schottky device which was characterised as not possessing a rectifying nature. Reasons for this were then explored such as poor contact-diamond adhesion, the diode possessing a smaller than expected Schottky barrier height, the I-V probes piercing the contacts or the depletion region width being too small to block carriers.

Acknowledgement

I would firstly like to thank my supervisor Professor Neil Fox for providing me this opportunity and for his help in seeing it through. I would like to express my deepest gratitude to Hugo Dominguez Andrade, James Smith, Robbie Mackenzie and Ramiz Zulkharnay for their help with many aspects of the project and getting me up to speed with all the different techniques used. I would also like to thank my fellow project students, Eduardo and Nathan for helping with discussions and growth runs.

Table of Contents

1	Introduction to Diamond power devices and their Growth	1
1.1	Project Specifications	1
1.2	How To Grow a Diamond	2
1.2.1	High Pressure, High Temperature Diamond Growth	2
1.2.2	Chemical Vapour Deposition Diamond Growth Categories	2
1.2.3	Hot Filament CVD	3
1.2.4	Direct Current plasma jet CVD	3
1.2.5	Microwave Plasma Assisted CVD	3
1.2.6	Evaluating diamond growth methods against requirements	4
1.3	Designing a Diode	4
1.3.1	Semiconductor materials and doping	4
1.3.2	PN and Schottky diodes	4
1.3.3	Crystallographic orientation	5
1.3.4	Considerations with CVD growth requirements	6
1.3.5	Finalising the Diode Design	7
1.4	Using the Microwave System	7
1.4.1	Reactor conditions	8
1.4.2	Sample preparation	8
1.5	Oxygen Terminations and Metallisation	8
2	Methods for Analysing Grown Layers	11
2.0.1	Raman Spectroscopy	11
2.0.2	Optical Microscopy	12
2.0.3	2-point Probe Resistance Measurements	12
2.0.4	Scanning Electron Microscopy	12
2.0.5	The Van Der Pauw Method	13
2.0.6	Hall Measurements	14
2.0.7	I-V Curve Measurements	14
3	Experimental Work	16
3.0.1	Getting accustomed to the reactor system	16
3.0.2	Working Towards Highly Conductive Boron Doped Layers	16
3.0.3	Analysis of layers (2) and (3)	17
3.0.4	Overview of Layer (4)	18
3.0.5	Analysis of layers (5) and (6)	18
3.0.6	Analysis of a hot filament grown layer	20
3.0.7	Growing the Intrinsic Layer	22
3.0.8	Analysis of the intrinsic layer	23
3.0.9	Preparation for Metallisation	23
3.0.10	Metallisation	23
3.0.11	Characteristics of produced devices	24

4	Discussion, Conclusion and Extensions	26
4.0.1	Different properties of oxygen terminated, (110) orientated diamond	26
4.0.2	Small depletion region width	26
4.0.3	Poor contact at the junctions	26
4.0.4	Piercing of the Contacts by the Probes	27
4.0.5	Tests and Treatments for Identified Problems	27
4.1	Conclusion	27
4.2	Possible Extensions	28

Chapter 1

Introduction to Diamond power devices and their Growth

Diamond is an astounding material. It possesses the greatest hardness of all known materials, exceptional thermal conductivity, strong hardness to radiation [2], a large dielectric breakdown strength and very high carrier mobility [1, 3]. For electronic purposes it is importantly a wide band-gap material with established methods for p-type doping and has found a strong position within electrochemistry [4] and power device applications [3].

One such use for diamond is within a beta voltaic device. By impinging diamond based Schottky diodes with energetic electrons from beta minus radiation, the ionising radiation leaves electron hole pairs within the semiconductor. These can then traverse the bandgap and can be collected, providing a current [5]. The present issue is that, currently, produced devices rely on an external radiation source or a layered semiconductor-radiation source structure, possibly more hazardous and less than ideal for bulk adsorption [5]. To remedy this, a method for growing diodes with

radioisotopes implanted such as C-14 or tritium is required. Doing so requires a full process for producing grown Schottky diodes which forms the subject of this dissertation.

Diamond based diodes may also find uses elsewhere: the high thermal conductivity serves as a great advantage in high performance computing, where removal of heat from key processing components is important for their longevity and efficiency [6]. Diodes and component layers can also find uses in cold cathode field emission displays [7], solar panels [8], radiation sensors [9] and temperature probes [10].

1.1 Project Specifications

For the application of beta voltaic devices, 2 main criteria must be met:

- The device as a whole must possess a low series resistance.

By reducing series resistance, less energy is lost to heat within the device, which is undesirable for a battery.

- The device should have good rectifying character.

Rectification is key to power applications; it simply wouldn't be a diode without it. This will maximise the current produced by the device, another desirable characteristic.

The following sections detail the initial design process for the device with respect to these conditions.

Material	Silicon	4H-SiC	GaN	Ga2O3	Diamond	AlN
Band gap / eV	1.1	3.3	3.4	4.9	5.5	6.1
Critical electric field / MV cm ⁻¹	0.3	2.8	3.5	8	7.7 to 20	10
RT mobility of holes / cm ² V ⁻¹ s ⁻¹	480	120	<100	N/A	2100 (bulk)	14
Thermal Conductivity / W m ⁻¹ K ⁻¹	150	370	100 to 253	11 to 27	2200 to 2400	253 to 319
Relative permittivity	11.8	9.8	9	9.9	5.5	8.5

Table 1: Electrical properties of wide and ultra wide band gap materials compared to diamond, in order of band gap size. Notice the large thermal conductivity and hole mobility at room temperature (RT) along with the critical electric field strength that diamond possesses versus the other materials. Sourced from Donato et al. and Umezawa et al. [1, 2]

1.2 How To Grow a Diamond

Diamond growth for most of history has been the realm of the extreme conditions available deep within the Earth's mantle: temperatures over 1000°C, pressures in excess of 10 GPa and a time scale over billions of years [11]. Obviously, such conditions would be difficult to recreate in a lab so other methods must be examined.

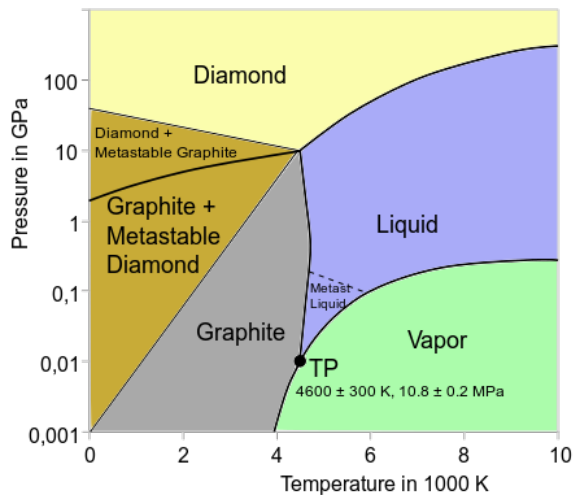


Figure 1.1: Phase diagram of carbon, attribution: Trackler (talk) 13:05, 18 July 2010 (UTC), Public domain, via Wikimedia Commons

1.2.1 High Pressure, High Temperature Diamond Growth

A significantly important method that is instead used is high pressure, high temperature (HPHT) diamond growth. In HPHT growth, diamond seeds and a carbon source are placed into a press and are heated to 1300 to 1600°C with a solvent metal or flux made from iron, nickel and/or cobalt [12]. The solvent acts to lower the temperatures required for diamond growth. The solvent metal will then melt, dissolving the hotter carbon source and transporting it to the colder diamond seeds where it will then precipitate onto them to form the HPHT diamonds [12]. This process can take days or weeks to complete [13]. This results in high purity and low crystalline defect density substrates but is limited to less than 1 cm² in most devices [14]. The process is, however,

expensive compared to the next category for thin films [15].

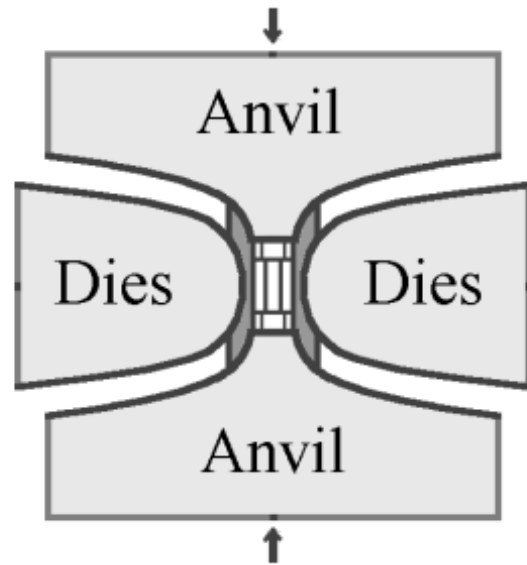


Figure 1.2: Diagram of a typical belt press HPHT cell, attribution: User:Hinonbey, Public domain, via Wikimedia Commons

1.2.2 Chemical Vapour Deposition Diamond Growth Categories

Alternative to this are the chemical vapour deposition (CVD) techniques such as hot filament (HF), microwave plasma (MW), direct current (DC), radiofrequency (RF), laser induced (LI) and chemical activation (CA) [16]. Most important to work in the diamond lab are HF, MW and DC CVD techniques.

All these techniques follow a similar pattern of operation:

1. Pumping of reactant gases into a chamber with the substrate (usually a methane/hydrogen mix plus, other gases).
2. Activating these gases through a technique specific means.
3. Adjusting growth parameters (the source gas ratios, substrate temperature etc.).

Key to the operation of CVD diamond growth is step 2, activating the source gases, and most important to this is the role of hydrogen (and/or oxygen) [17]. Activated hydrogen takes on 3 roles: firstly, it terminates the “dangling” bonds

of the carbon atoms on the surface. Next, it can cleave apart neutral molecules such as the methane or CH bonds on the surface to produce reactive radicals. Finally, the hydrogen acts to prevent the formation of graphite on the substrate [16]. This property is due to the etching rate of atomic hydrogen being much greater on sp^2 hybridised graphitic carbon than on diamond like sp^3 carbons. Overall, this gives a good selectivity for only the growth of diamond under the right conditions.

The following sections examine the methods of activation with the most relevance to the equipment in the diamond lab.

1.2.3 Hot Filament CVD

In this method, a filament is strongly heated at a distance a few millimetres away from the substrate on a cooled stage. In [18], Lai et al. uses a filament temperature between 1700 and 2000°C with a filament to substrate distance of 2 to 4 mm for example, though hotter set ups can be found such as in Manawi et al. [19]. These high temperatures lead to the activation of atomic hydrogen in the gas mixture, kick-starting growth. This process has a three main drawbacks being contamination from the filament, and its degradation, and the low growth rate between 1 and 10 $\mu\text{m h}^{-1}$ [16]. However, the technique is relatively inexpensive to setup, provides high quality diamond layers and can operate over very large areas up to 100,000 mm^2 [16].

1.2.4 Direct Current plasma jet CVD

Under this method, the source gases are passed between two electrodes. A voltage is applied between the electrodes, and charge carriers are accelerated between them. Initially, only a small current travels the gap, ionising gas molecules through impact ionisation. With increasing voltage over the striking voltage, a plasma begins forming and increasing in size. When the plasma has covered the whole electrode and the voltage is further increased, the electrode will heat up. This begins thermal emission of charge carriers, eventually leading

to an arc discharge, characterised by high current and low voltage. This arc discharge acts as a plasma "jet" for deposition [16, 20]. DC plasma jet CVD has a middling growth area at 100-10000s of mm^2 and possibly the fastest linear growth speed with a record at 930 $\mu\text{m h}^{-1}$ [21]. The system is generally used to produce large (20 cm diameter) high quality, free-standing diamond films. However, this comes at the cost of an expensive chamber, risk of contamination from the electrodes, low control and very high power consumption [16].

1.2.5 Microwave Plasma Assisted CVD

Another method of striking a plasma for activation is to use electromagnetic waves. Initially, photons will impinge the neutral gas mixture in the chamber at microwave frequencies, heating it slightly due to dielectric heating and multiphoton absorption [16, 22]. By tuning the frequency to a factor of 10 less than the resonant frequency of the molecule vibration/rotation (chosen to increase penetration depth [22]) the adsorption can increase the energy of the molecules and, eventually, ionise them. Once ionised, new mechanisms become available such as free-free absorption and ohmic heating. A ball of plasma can now be formed above the sample through careful design of the chamber dimensions [16].

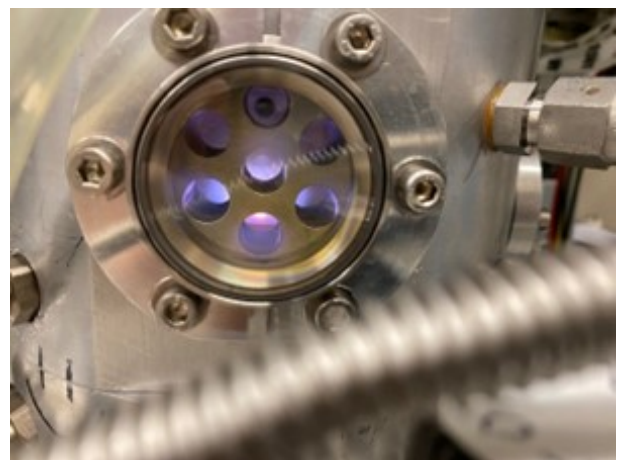


Figure 1.3: Photograph of the boron chamber during a growth run

MW CVD offers comparable maximum

deposition areas to DC and HF CVD with very high diamond layer quality. The system possesses an intermediate growth rate from 0.1 to 34 $\mu\text{m h}^{-1}$ and an intermediate running cost as well [16].

1.2.6 Evaluating diamond growth methods against requirements

Comparing the methods to the requirements yield a few obvious conclusions: HPHT would be unsuitable for this project. It's expensive and time intensive procedure would not yield results in the required time frame, though previously grown HPHT diamonds can serve as good substrates for growth. The three outlined CVD methods all provide acceptable avenues for the project however the intermediate growth rate and cost of MW CVD along with its superb quality films appears to be most useful for the growth. A useful comparison for the results however would be between these systems, so a HF CVD will be examined as well.

1.3 Designing a Diode

Diamond is a semiconductor possessing a very wide band gap and as such exhibits useful electronic properties. The following sections provide detail into semiconductor materials, doping and diode structure.

1.3.1 Semiconductor materials and doping

Semiconductors are materials where the Fermi level, the energy to add one electron to the bulk, lies in a region between energy bands, lying above the valence band (VB) and below the conduction band (CB) [23]. For very small band gap semiconductors, thermal excitation can take electrons from the VB to the CB, though for wider band gap materials, this isn't possible [23]. Semiconductor materials can be doped with heteroatoms to change the relative position of the Fermi level with respect to the VB and CB [23]. By introducing an impurity with less valence electrons, such as boron for a carbon semiconductor, a new acceptor (hole)

energy levels can be introduced, moving the Fermi energy very close to the VB. This allows for conduction of electrons to the new acceptor levels [24]. This is p-type doping. There is likewise a similar case for n-type doping, adding an impurity with more valence electrons to create donor levels near to the CB [23].

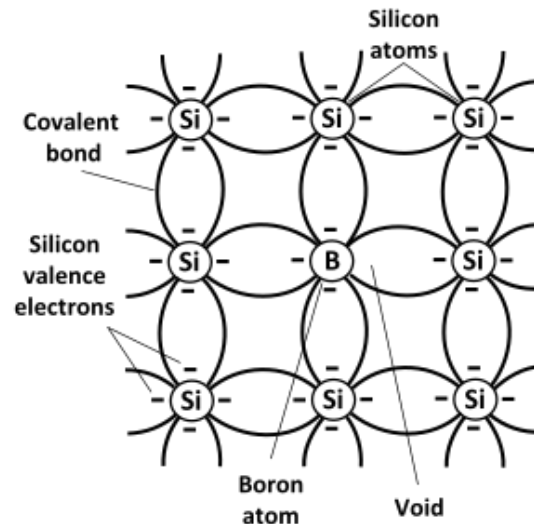


Figure 1.4: Diagram illustrating boron doping of, in this case, silicon. Boron has 1 less valence electron so contributes a hole. Attribution: Michel Bakni, CC BY-SA 4.0 <https://creativecommons.org/licenses/by-sa/4.0>, via Wikimedia Commons

When two semiconductor materials are placed in contact with one another, their chemical potentials or Fermi levels will equalise, but this causes the CB and VB to bend, producing a built-in potential. This can be viewed through the creation of a depletion region [24]. Mobile carriers will travel from one side to the other, electrons filling holes and vice versa, creating a region of filled holes on one side and removed electrons on the other near the interface [24].

1.3.2 PN and Schottky diodes

The depletion region will form an electric field at equilibrium with the filled holes giving a net negative charge on one side and the removed electrons a net positive on the other side. This region will inhibit further electron transport and current, unless the applied potential difference

acts to assist them across the gap. The reverse direction will increase the field strength across the depletion region, further inhibiting current. This provides the key effect of diodes, rectification, the process of only allowing charge to flow in one direction across the device. This process is best illustrated in PN junctions, the combination of a p-type doped material with an n-type doped material. Here, if the applied voltage goes from the P to the N side, electrons will travel from the N side to the P side, reducing the depletion region. But, in the opposite case, electrons will attempt to flow into the N type region, contributing to a greater opposing field in the device [24].

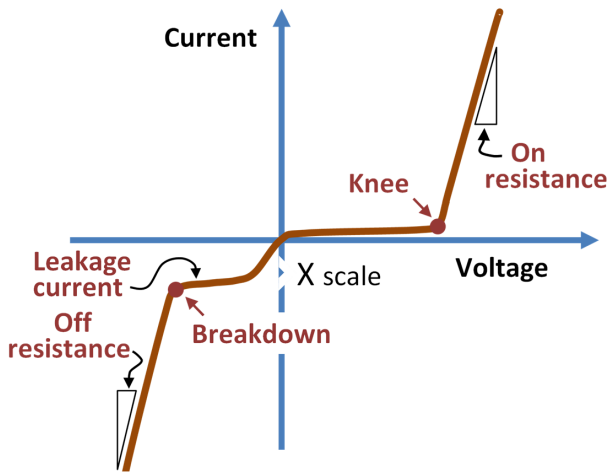


Figure 1.5: Diagram of a non-ideal I-V curve of a diode, attribution: Brews ohare, CC BY-SA 3.0 <https://creativecommons.org/licenses/by-sa/3.0>, via Wikimedia Commons

This likewise can occur in metal-semiconductor junctions. For p-type semiconductors, the work function of the metal (the energy required to remove an electron from the bulk to vacuum) must be less than the work function of the semiconductor for a rectifying junction to form [24]. The opposite holds for n-type materials. Following the same fermi level rule as before at equilibrium yields a depletion region in the semiconductor near the interface. This creates a so called Schottky barrier, an energy barrier to cross from one side to the other. For p-type-metal junctions, the forward direction for electrons is from the metal to the semiconductor (with the potential difference applied the other way) and the opposite for

n-type junctions. For p-type materials, the barrier height is found as the band gap of the semiconductor plus its electron affinity (the energy to add one electron from vacuum to the CB) minus the metal work function. For n-type it's given as the work function of the metal minus the electron affinity of the semiconductor. To create a full diode with a Schottky junction, it is key to have one contact on the device be ohmic, as in not fulfilling the condition for a Schottky junction [24]. Generally, this is achieved by using different metals on either contact.

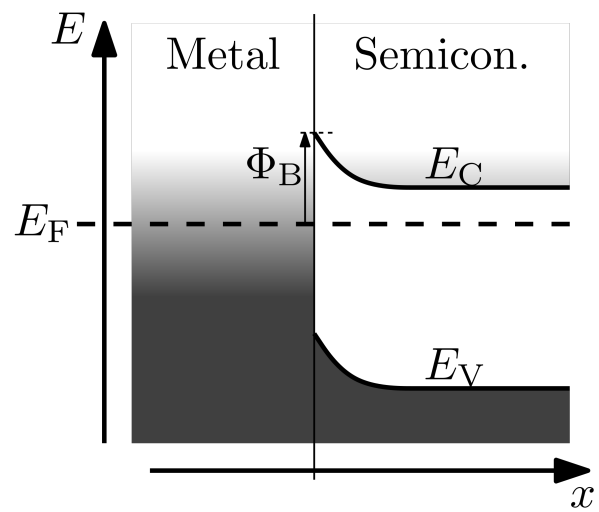


Figure 1.6: Band diagram of a Schottky junction forming a barrier, attribution: Nanite, CC0, via Wikimedia Commons

This means that when designing a Schottky diode, several variables must be tracked. Doping, crystallographic orientation and surface atoms present can all affect the work function of the semiconductor. A note here is that the Schottky barrier height may be independent of the metal work function such as during Fermi level pinning where the surface states dominate [24].

1.3.3 Crystallographic orientation

Diamond as a crystal assumes a face-centred cubic (FCC) lattice structure with a basis of two carbon atoms per site. This tetrahedrally, tight-bonded structure gives rise to many of the exceptional physical properties of

diamond [25]. Crystals may be cleaved along planes of high symmetry, denoted by Miller indices (hkl) where h,k,l are the reciprocal of the plane's intersection with the x,y,z axes respectively. Through cleaving, a surface is formed, described by a net. The surface net structure is important as it can require different growth conditions to other possible surface structures alongside its affect on the work function [25].

With the growth of single crystal CVD diamond, the orientation of the substrate should remain the dominant direction of the grown layers, with some facets forming at the edges and corners with different directions [26]

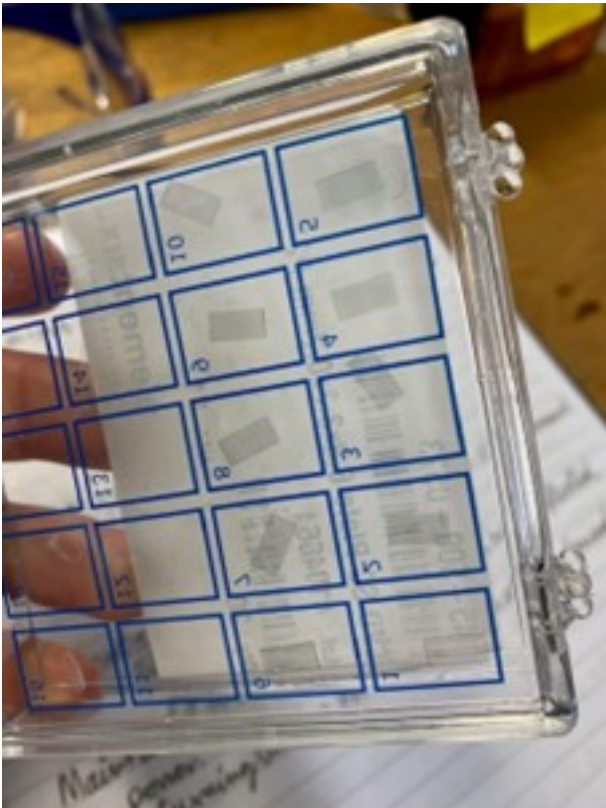


Figure 1.7: Photograph of the substrates available for the diodes. They are 3mm by 6mm (110) HPHT diamond chips from Element-6.

For this work, the specifications called for sample dimensions only available in (110) orientated substrates so this orientation formed the base of the diode. (110) orientated diamond surfaces are shown to possess higher C-H bond densities compared to other directions, leading to higher sheet carrier densities and thus lower sheet resistance [27].

1.3.4 Considerations with CVD growth requirements

One requirement of the diode device is the ability to dope layers with donor or acceptor dopants. In the case of diamond, boron is a widely used dopant to achieve a p-type layer [28, 29] and can be introduced in a gas, such as diborane, into the reaction mixture. N-type diamond on the other hand has been a long running problem for research. Commonly used donor dopants can distort the lattice or possess donor levels too deep for good performance at room temperature [30]. This means only p-type diamond is truly feasible for this project, so the diode must be of Schottky design. Boron doping does present some issues however. The boron source gas, diborane, reacts readily with oxygen to form solid boric oxides [31]. The produced solid generally appears as a white powder and can cause problems, such as blockages, if formed within the gas pipes. This is mitigated using a long, coiled length of pipe before the line connects to the reactor to prevent formation of the solid near the gas board and to localise formation to an easy to access section of pipe. Boron will also cling and stick to the reactor chamber walls between runs, meaning that chambers that have done one boron run are now contaminated with the material. This can lead to unintentional doping of materials, though this can be used for the creation of very lightly doped layers as well [32].

CVD growth of single crystal diamond is homoepitaxial, carbon atoms are “placed” layer by layer onto a substrate [26]. This means any diode structure must be constructed in a vertical format, with the original substrate as a base for non-free standing films. This leaves pseudo vertical Schottky barrier diode structures as the most viable compared to the alternative vertical structure. In this design, the conductive, doped p-type layer (p-layer) is first deposited over the surface of the substrate. Then a section towards the end of the device is masked off, and the, very lightly doped, intrinsic layer (i-layer) is grown only to cover the remaining area [29, 28]. With both layers in place, an ohmic contact can be deposited on the exposed section of the p-layer and a Schottky contact on the i-layer.

Such contact deposition can be done using a metal evaporator.

1.3.5 Finalising the Diode Design

With all this in mind, contact metals can be chosen. For the Schottky contact, aluminium and gold are popular choices as both regularly present a Schottky barrier equal to or greater than 1 eV for p-type, oxygen terminated diamond [33, 34]. There is a caveat however that little research has been done into the particular case of oxygen terminated (110) orientated boron doped diamond. This is further complicated by oxygen terminations possessing two main arrangements, ketone and ether, on the diamond surface, both with different electron affinities [35]. Diamond is well known to possess a negative electron affinity under certain conditions [36, 37], it's possible that the Schottky barrier height may be significantly reduced by this. However, generally oxygen terminations lead to an increase in electron affinity [37].

Previous work in the diamond lab utilising aluminium/gold contacts have also utilised a nichrome/gold ohmic contacts, owing to the barrier asymmetry and thus built in voltage they would produce [34].

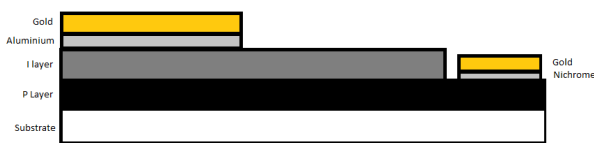


Figure 1.8: Example diagram of the pseudo vertical diode structure. Layer darkness denotes desired doping level with the darkest layer (the p-layer) being the most doped.

The thickness of the layers is important for tuning electrical characteristics. A wider p-layer will have a lower length-ways end to end resistance, a wider i-layer could give a greater break-down voltage for the device. Targeting specific layer thicknesses is difficult as there was no procedure for growing on (110) orientated diamond initially, so no growth rate

analysis had yet been conducted. The metal contacts only need to be thick enough for probes to be placed onto them for I-V measurements, 10 nm of metal followed by 100 nm of gold was proposed to achieve this.

1.4 Using the Microwave System

The first goal of the project was to synthesise and characterise diamond films grown on single crystal diamond substrates. Most useful to the diode project would be working towards highly boron doped, conductive layers. The HF reactor in the diamond lab is already able to produce layers with length-ways end to end resistance of around 600 Ω . This level serves as a goal for MW grown samples to allow for direct comparison between diodes constructed out of either method.

Operation of the microwave system went as follows :

1. The chamber was brought to room pressure by opening the venting valve and the stage lowered.
2. A spacer wire of experiment specific thickness was placed into the centre of the chamber followed by a molybdenum substrate holder.
3. The substrate is then placed centrally on top of the holder and necessary masks put in place.
4. The stage is raised, and the system roughly pumped down followed by activating the turbopump to bring the system down to vacuum. Water and air cooling is activated.
5. The mass flow controllers for the desired input gases are then set with their valves open on the gas board. Hydrogen is flowed into the chamber at around 50 Torr.
6. Microwave power is then set to 4.7 kW and switched on, sometimes the plasma is successfully struck just above the sample here.

- (a) If struck in a different location, switch off the apparatus and try again.
 - (b) If no plasma is struck, adjust the tuning knobs until a plasma is struck.
7. Bring the reflected power to approximately 0 using the tuning knobs.
 8. Switch on the other MFCs and bring the chamber pressure and power up to experiment conditions, keeping an eye on the plasma so it does not extinguish.
 9. Observe the reactor for the required experiment time.
 10. Switch off the systems safely and retrieve the final sample, returning the reactor to its empty pumping down state.

1.4.1 Reactor conditions

Reactor parameters can be measured on several devices such as the different range pressure gauges, the forward and reverse power gauges and the temperature from the system's pyrometer. This ensures a relatively consistent set of conditions between runs. The system's spacer wire is also important as the thicker the wire, the less contact between the substrate holder and the cooling stage, so the temperature of the sample is increased for lower input microwave power. The pyrometer, if aligned on the sample and set to the correct material emissivity, provides a good estimate of the temperature of the substrate but is liable to moving. Masks may also interfere with its operation, possibly leading to it not giving any reading. "Recipes" for layers come primarily from the ratio of gas flow rates into the reactor. These input gasses are usually methane, hydrogen and diborane though nitrogen and oxygen can be used for particular applications. Important to this project is the ratio of methane to hydrogen gas molecules and the ratio of diborane to methane molecules. Care must be taken as the diborane gas cylinder is diluted to 100 ppm of diborane in hydrogen. Small variations in parameters can rapidly change the growth process. For instance,

the forward microwave power determines the concentration of hydrogen ions in the plasma and thus the rate of growth and, indirectly, the layer quality. Increasing the methane to hydrogen ratio has a similar effect, decreasing it can lead to pits forming on the layer surface. Substrate temperature and input microwave power can also seemingly change the dominant growth mechanism from homoepitaxial growth to secondary nucleation in some experiments.

1.4.2 Sample preparation

Growth may be performed on many different samples given correct preparations. Silicon wafers can be manually abraded with fine diamond powder to provide nucleation sites or treated with an electrospray of diamond nanoparticles. Growing on materials other than diamond presents challenges due to the mismatch in thermal expansion coefficients of the materials and lattice parameters, which can lead to stresses, fractures and defects forming during heating, cooling and growth [38]. Growth conditions may also vary greatly from substrate to substrate.

For single crystal growth, diamond substrates are the most appropriate. These are generally HPHT grown and polished. All substrates for the microwave reactor are cleaned via an acid wash to remove metal contaminants and sonicated in acetone for 10 minutes to remove any residues. One important precaution is the use of gloves during handling and the use of non-metal tweezers during transfer to avoid contaminating or damaging the substrates.

1.5 Oxygen Terminations and Metallisation

Metallisation for the placement of contacts was done using an Edwards evaporator system. This system allows for the loading of two metal sources in the chamber simultaneously, allowing for quicker deposition of the metal-gold contacts desired. Prior to metallisation, the surface needed treatment to become oxygen terminated.

Two methods were possible: exposure to an

oxygen plasma or the use of a UV ozone cleaner. The oxygen plasma would be provided through a modified sputter coater, however this method may lead to etching of the diamond surface, possibly reducing layer quality. The UV ozone cleaner on the other hand presents a gentler method.

The device used was a Jelight UVO cleaner (model No. 42A-220). Using UV lamps, the device decomposes oxygen molecules and synthesises them into ozone, which is then further decomposed into activated oxygen atoms. These activated atoms can then oxidise the surface and react off any organic contaminants. Samples are simply placed onto the device's tray, with the side of interest facing up, and treated for 20 minutes. Samples should now be ready for metallisation.



Figure 1.9: Photograph of the UV ozone cleaner used.

The evaporator system generally begins pumped down to high vacuum to prevent contamination, so the device is brought back up to room pressure and the shield and bell jar of the device twisted off. From here metals can be loaded, whilst wearing gloves:

- If using rod as the metal source, a coil shaped filament is required.
- If using thin wire, bundle it into a ball and place into a boat shaped filament.



Figure 1.10: Photograph of the evaporator system. Loaded in the coiled filaments is gold on the right and aluminium on the left.

When loading multiple metals, a barrier can be placed between the source locations to prevent contamination. The sample can then be placed onto the stage, ensuring that there is direct line of sight from the metal sources to it. The sample should also be the same distance from the sources as to the thickness monitor, to ensure accurate thickness measurements. Appropriate masks can then be placed on top of the sample. The jar can then be replaced, along with the shield, and the system pumped down to operating pressure of 10^{-6} mbar in two stages: 1st a roughing pump down to 6.0×10^{-2} mbar or below, followed by the vacuum pump. The pumping procedure takes approximately 2 hours. For the desorption of water, the stage can be heated to 250°C 1 hour before coating. To measure the thickness of the deposited

coating, a crystal-film thickness monitor is used. Densities of deposited metals are entered into the device. By measuring the change in frequency of an oscillating quartz crystal and comparing that to the inputted density, an estimate for the thickness of the deposited coating is outputted on the device's display.

Deposition can now begin by selecting the desired metal source and slowly increasing the input power. This power must be increased slowly as the source needs time to heat to equilibrium. At high enough power, the source metal will melt and wet the filament. The source may start to sag during operation, to prevent it falling the power can be decreased and slowly increased again to encourage wetting of the filament. At further powers, the thickness monitor will begin to show an increased thickness, a comfortable rate of growth can then be established with further power adjustments. As the device is non-directional, metal will begin to coat the bell jar as well. As the desired thickness is approached, the power can be reduced and set to 0 by pressing the "trip" button.

The chamber can then be slowly brought back to room pressure (and cooled to room temperature) and the newly coated samples retrieved.

Chapter 2

Methods for Analysing Grown Layers

Several methods are available for analysis of layers such as Raman spectroscopy, imaging with an optical microscope, utilising a scanning electron microscope (SEM), 2-probe resistance measurements and Hall/I-V measurements. The following sections detail the principles behind the techniques and their methods.

2.0.1 Raman Spectroscopy

A popular technique for diamond analysis due to the material's characteristic peak at 1332 cm^{-1} [39], Raman spectroscopy is a technique that relies on the inelastic scattering of laser light in a sample [40]

For absorption of a photon to occur, the new state (rotational/vibrational/electronic) must exhibit a change in the molecule's polarizability, with the magnitude of the change being proportional to the Raman scattering [40, 39] This absorption leads to a Raman shift of the photon's frequency (and energy) which can be measured by the spectrometer alongside the scattering intensity to yield the final spectrum.



Figure 2.1: Photograph of the Raman spectrometer in use. Samples are loaded onto the stage, focused with visible light then illuminated with laser light to take the spectrum.

Important to this work is the technique's ability to discern several impurities in grown layers such as graphite or boron dopant atoms. The full width half maximum (FWHM) of the diamond peak at 1332 cm^{-1} is also regularly used as an indicator of diamond layer quality; a larger value indicates polycrystalline phases and thus is of lower quality [39]. Another effect is that the diamond peak is seen to shift lower for increasing boron content [41], a giveaway for approximately comparing boron concentration in samples. The method for using the Raman device is as follows:

1. Turn on the laser, for this project a green laser with a wavelength of 514nm was used.
2. In optical mode, place the sample on the microscope carriage and begin moving the stage up. The device possesses an octagonal focus guide that comes into sharp focus at the correct stage height.

3. Switch to laser light and begin adjusting accumulation settings, the goal is to maximise height without saturating the collector.
4. Centre the collection at the diamond peak (1332 cm^{-1})
5. Collect the spectrum, store it as a csv and transfer it to origin to fit Gaussian(s) curves to the data.
6. Using the Gaussian fit, find the FWHM of the data peak(s) and the peak positions.

2.0.2 Optical Microscopy

Several surface features are visible using an optical microscope, allowing for quick comparison between surfaces. This technique can also provide hints to the growth mechanisms present such as visible and frequent “bumps” for secondary nucleation or a relatively featureless surface for homoepitaxial growth. Some colouration patterns can also be visible; boron doped samples generally appear darker at higher boron concentration so that darker areas of the sample may hold the greatest concentration of boron. It could also be indicative of graphitic carbon or other impurities.

In terms of method, the optical mode of the Raman device was used, given the same steps for 1 and 2 and the images taken with just a phone camera, pointed down the view ports.

2.0.3 2-point Probe Resistance Measurements

Although a trivial method, this technique provides very quick feedback into the electrical properties and thus possibly the dopant concentration in a layer. With increased dopant concentration, more mobile carriers are present in the sample at room temperature so the conductivity should increase and the resistivity decrease [23]. Note that this method specifically measures resistance, thicker layers will give smaller values by virtue of their dimensions only, and not due to a decreasing resistivity. For like-to-like comparisons it

is thus best to only compare samples of the same dimensions, only with different known thicknesses. The method is as follows:

1. Place sample onto the stage and move it underneath the gold probes.
2. Using the camera for guidance and the tuning knobs for accuracy, adjust the probes until just touching the top of the sample at the thin ends.
3. Move the probes toward the centre and edge of the thin ends of the sample and record the resistance.

Not all layers give sensible readings for this technique (such as poorly doped layers) so only the 1st digit and the order of magnitude was needed for rough comparison. The apparatus can also be used to find the I-V curve of the final diodes by applying a small voltage across the contacts and measuring the current produced.



Figure 2.2: Photograph of the 2-point probe system in use. Probes are placed as far away from contacts as possible to ensure equal measurements between runs.

2.0.4 Scanning Electron Microscopy

Of the techniques, SEM by far has the greatest resolution in real space. This technique allows for μm scale images of the surface (down to nanometre scales on some devices), allowing for determination of layer heights (on the order of 1 to 10 μms) and visualising any surface diamond grains.

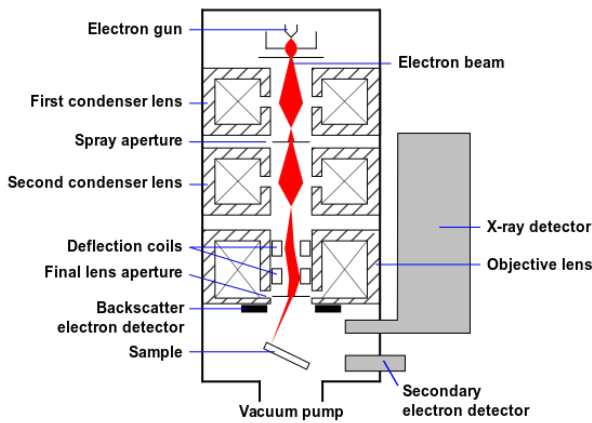


Figure 2.3: Diagram of a typical SEM device's setup. Attribution of File:Schema MEB (it).svg: User:Steff, modified by User:ARTEderivative work MarcoTolo, CC BY-SA 1.0 <https://creativecommons.org/licenses/by-sa/1.0>, via Wikimedia Commons

For this technique, electrons are produced generally through heating and thermionic emission from an electron gun [42, 43]. These electrons are focused using electromagnetic lenses onto a sample in high vacuum. Electrons in the sample are excited, emitted and detected. These secondary electrons have small energies on the order of 50 eV, giving a short mean free path in the sample. This means that most detected electrons are thus only from the sample's surface where now the topology of the surface can be resolved [43]. The device can then rasterise the whole target area, scanning across it to output an image. Image brightness is generally proportional to the electron energy, so for more conductive parts of the sample, it can appear brighter. This can also be the case for sharp edges and corners, allowing for visible depth in the image. For non-conductive samples, impinging electrons may charge the surface, leading to the imaged target area getting brighter and brighter with further scanning, reducing the contrast between features. As all samples in this project should be conducting to some degree, no sample preparation is required though, the usual step is to coat them in a very thin layer of conductive material such as gold [43].

Typical usage as follows:

1. Choose samples to load, 7 at a time

maximum, and load them onto conductive carbon tape topped specimen stubs to be placed onto the carousel.

2. Begin pumping down the chamber and heating the electron gun.
3. Once ready for operation, set the position to the first stub and focus to give a clearer image.
4. Proceed to the sample's sites of interest (edge, corner, surface features). Reduce the scanning speed and adjust the contrast and brightness to give a clear image of the feature. This image can then be saved.

NOTE: If looking at the layer heights, move the stage down and begin tilting it. Finding a layer facet in the same plane as the image is best. Take an image and use the scale to give the facet height, correcting based on tilt angle and facet angle to give the layer height.

5. Other samples can then be examined, though refocusing may be required.

2.0.5 The Van Der Pauw Method

Required for discussion of Hall measurement techniques is the, commonly used in conjunction, Van der Pauw method for finding the sheet resistance and sheet carrier density [44]. In this method, a simply connected sample is connected to electrode at its corners numbered 1,2,3,4 anticlockwise around the sample. Two characteristic resistances of the sample can be found, $R_A = V_{43}/I_{12}$, V_{43} the potential difference measured from 4 to 3 and I_{12} the DC current applied into 1 and out of 2, and $R_B = V_{14}/I_{23}$ with similar definitions for V_{14} and I_{23} . These are related to the sheet resistance R_s by

$$\exp(-\pi R_A/R_s) + \exp(-\pi R_B/R_s) = 1 \quad (2.1)$$

which then must be numerically solved for R_s . For known layer heights, the bulk resistivity, ρ , can then be found as $\rho = R_s d$ where d is the layer thickness [44].

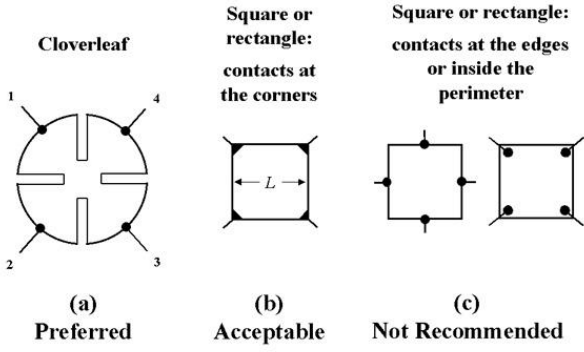


Figure 4

Figure 2.4: Diagram of contact placement during Hall and Van der Pauw measurements via NIST. As rectangular samples are used, corner contacts provide the least error.

2.0.6 Hall Measurements

Hall measurements rely on the eponymous Hall effect [45]. In a magnetic field, electrons (of charge, $q = -e$), with some velocity \underline{v} , will experience a force, \underline{F} , given by the Lorentz force: $\underline{F} = q\underline{v} \times \underline{B}$. For electrons flowing as a current within a perpendicular magnetic field, this causes a charge imbalance across the width of the conductor, creating a potential difference known as the Hall voltage. This Hall voltage V_H has magnitude equal to $IB/(qnd)$ where I is the current, n is the bulk carrier density and d the conductor thickness (parallel to \underline{B}). Alternatively, the sheet carrier density n_s can be used, $n_s = nd$, giving [23]

$$n_s = IB/(q|V_H|) \quad (2.2)$$

In the Van der Pauw setup up under a magnetic field parallel to the film normal, V_H can be found by applying a current to contact 3 to 1 and V_H measured at the potential difference V_{24} . Thus, by using both methods, the bulk carrier concentration can be found, allowing for estimation of the dopant concentration. Usefully, the sign on V_H under this setup will reveal the majority carrier and so, the type of the semiconducting layer. For p-type, V_H should be positive and for n-type, V_H should be negative. Another important metric is the carrier mobility found as

$$\mu = \frac{|V_H|}{R_s IB} = \frac{1}{qn_s R_s} \quad (2.3)$$

which relates bulk carrier concentration to conductivity [23] For Hall and Van der Pauw measurements, a Ecopia Hall effect measurement system was used (HMS-5000). The operating procedure proceeds as follows:

1. Remove the stage from the device and place into supporting structure.
2. Place sample, grown side up, onto the stage and manoeuvre the electrodes to the corners of the structure. Error is proportional to the distance of the contact from the respective corner of the device, so these are placed as far into the corners as possible.
3. Tighten down the contacts and return the stage to the device.
4. Enter the layer's thickness into the connected software.
5. Measurements can now be started on the software loaded onto the device's connected computer, applied current and voltage ranges can be changed to give a range of measurements; these measurements should be concordant.

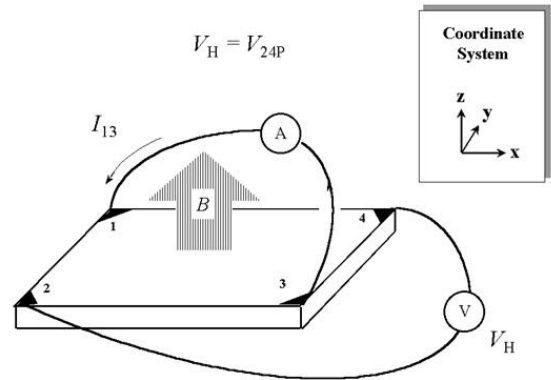


Figure 3

Figure 2.5: Diagram showing which corners the voltage and current are applied and measured between via NIST.

2.0.7 I-V Curve Measurements

I-V curve measurements allow for finding the operating constraints of diode devices such as breakdown and “knee” voltages. For an ohmic

device such as a resistor the current through the component is expected to be the applied voltage divided by the resistance of the component. Diodes on the other hand exhibit a nonlinear relationship. For a forward biased diode in equilibrium, the Shockley diode equation states that the diode current,

$$I_D = I_S \left(\exp\left(\frac{V_D}{nV_T}\right) - 1 \right) \quad (2.4)$$

where I_S is the reverse bias saturation current, V_D the voltage across the diode, V_T the thermal voltage = kT/e and n an ideality factor that regularly varies from 1 to 2, though $n = 1$ is the ideal case [46, 24]. For component resistance limited current, models generally place a resistor in series with a device obeying this diode law. By applying voltages in a range greater than the thermal voltage (around 25mV at 300K), the curve should be seen to rise. For reverse bias operation, some minority carriers (such as electrons in p-type materials) will be able to cross the depletion region, giving a small, so called leakage current [24] This leakage current will rise very slowly with increasing reverse bias until a breakdown voltage is reached [24]. At this point, small increases in reverse bias led to large changes in current as the rectifying nature of the diode ceases. This behaviour is driven by three main mechanisms: the Zener breakdown, avalanche multiplication and tunnelling. Highly doped materials generally experience Zener breakdown where increased reverse bias leads to a large magnitude electric field across the physically thin depletion region. Large electric fields can break down covalent bonds in the material, releasing electron-hole pairs giving rise to a rapid rise in reverse current [24] For avalanche breakdown in less doped materials, the depletion region is wider, giving a higher breakdown voltage, so carriers crossing the depletion region are accelerated greatly. These carriers can then collide, breaking bonds and creating electron-hole pairs. These new carriers can likewise collide, giving an avalanche of new carriers, giving a sharp increase in the reverse current [24]. In tunneling, current is able to tunnel through the thin but large barrier, generally occurring for small band gap materials and at higher temperatures [24]. The

breakdown voltage can be changed through diode design by introducing an undoped/very lightly doped layer (an intrinsic/p- or n- layer), effectively increasing the depletion region's width and lowering the max electric field during regular operation, reducing the chance of breakdown.

The Knee voltage of a diode is the voltage in the forward direction where small increases in voltage lead to much larger changes in current. This is the voltage required to overcome the built in field of the diode's depletion region and is a material specific parameter [24].

Chapter 3

Experimental Work

During the timeframe of this project, myself and 2 other final year students were working on the same reactor for different boron doped diamond projects. This meant reactor time was divided between us, though most work was done in pairs to oversee each other's methods and to ensure that someone is always available to keep watch during growth runs. We all shared the similar first goal of growing a conductive boron doped layer on single crystal diamond so the following sections will feature some of their results, with appropriate accreditation. This is done to provide a fuller view of the process we went through in finding an appropriate growth procedure for the boron doped layers. Likewise other lab users were also working to similar goals at the time.

3.0.1 Getting accustomed to the reactor system

The first task was to become familiar with the microwave system and to establish what conditions seen in literature were transferable to this reactor. This began with a series of induction and training sessions with Dr Hugo Dominguez Andrade. Likewise, similar inductions took place for different silicon substrate nucleation methods and the Raman system.

The microwave system controls gas flow into the chamber using a series of mass flow controllers that could be set to a range of values with units of Standard cubic centimetres per minute (sccm), as in the flowrate in cm^3/min under standard temperature and pressure. This means the flow rates are proportional to the concentrations of the gases in the chamber, allowing for calculation of the methane to

hydrogen ratio ($[\text{CH}_4]/[\text{H}_2]$) and the boron ratio ($[\text{B}_2\text{H}_6]/[\text{CH}_4]$) directly. The chamber was generally operated in pressure ranges between 90 and 150 Torr, forward microwave power between 1.25 and 1.9 kW and a total gas flow rate of up to 1000 sccm.

For the first growth run, a manually abraded silicon square was used. Following the microwave procedure, the chamber was opened and the 0.1mm spacer wire placed in followed by the molybdenum holder and the sample. Initially, 1.5kW and 150 Torr was tried as the conditions, however this led to a temperature over 1100°C , too high for diamond growth on silicon, so the conditions were lessened to 1.20kW and 120 Torr to give a temperature of 1035°C . This was grown for 1 hour. After 30 minutes, the conditions had to be readjusted as the forward power had drifted up to 1.23kW. In all future runs, the reactor chamber was readjusted at least twice an hour to prevent this drifting during longer runs.

After one hour the sample was removed, and by quickly checking under the Raman system, was confirmed as giving the 1332 cm^{-1} peak implying the presence of diamond.

3.0.2 Working Towards Highly Conductive Boron Doped Layers

Below is a table of all the different trialled conditions for growing boron doped layers on (110) single crystal diamond substrates in chronological order. Conductive layers are layers with a measurable resistance and are numbered for referencing later in the text.

When the samples first arrived in the lab, conditions that have previously worked on other single crystal substrates were tried. These formed the initial 3 runs by Dr Hugo Dominguez Andrade where a boron doped layer was attempted to be grown underneath a mask. The first two runs were viewed as failures though 3rd run, layer (1), possessed a measurable resistance of $130\text{ k}\Omega$. At a $[\text{B}_2\text{H}_6]/[\text{CH}_4]$ ratio of 100ppm, more boron could be added to the mixture to hopefully lower the sample resistance. A notable feature was that the grown layer featured a pitted

surface when viewed under a microscope, expected to have been caused by the low (0.2%) [CH₄]/[H₂] ratio of the run. These conditions provided the basis for future runs where some growth parameters could be

varied to try to find a procedure for growing a more conductive boron layer. However, the methane ratio was increased to 1% for all future runs to reduce pitting.

Temperature / °C	Spacer wire diameter / mm	Pressure / Torr	Forward power / kW	[CH ₄]/[H ₂]	[B ₂ H ₆]/[CH ₄] / ppm	Time / hours	Conductive?
9.23E+02	2.28E-01	1.20E+02	1.50E+00	4.35E-02	1.00E+02	1.00E+00	No
1.10E+03	2.28E-01	1.20E+02	1.20E+00	4.35E-02	1.00E+02	3.00E-01	No
1.10E+03	2.28E-01	1.00E+02	1.86E+00	2.00E-03	4.00E+01	1.00E+00	Yes (1)
8.70E+02	2.28E-01	1.20E+02	1.73E+00	9.88E-03	4.08E+01	2.00E+00	Yes (2)
1.08E+03	2.28E-01	1.20E+02	1.88E+00	1.02E-02	2.44E+02	1.00E+00	Yes (3)
8.70E+02	2.28E-01	1.00E+02	1.86E+00	1.01E-02	5.00E+02	1.00E+00	Yes (4)
1.09E+03	5.00E-01	95-100	1.35E+00	1.01E-02	6.67E+02	2.00E+00	Yes (5)
1.09E+03	5.00E-01	95-100	1.35E+00	1.01E-02	6.67E+02	4.00E+00	Yes (6)

Table 3.1: Growth runs conducted to find a procedure for growing Boron doped diamond on single crystal (110) diamond substrates. I ran or assisted the growths of layers 2, 3, 4, 5 and 6.

3.0.3 Analysis of layers (2) and (3)

Layers (2) and (3) both appeared identical and shared many similar results so are treated simultaneously here. Layer (2) was grown with the motivation of looking at lower temperature conditions and layer (3) for higher pressure conditions. This meant that layer (2) was also grown at lower forward microwave power, so the pressure was increased to somewhat maintain the microwave power density.

Both samples produced from the growth runs appeared identical to how they went in: colourless, clear samples. However, under the optical microscope they revealed a frequent pattern of bumps over their surface. Layer (2) had a measurable resistance of 60 kΩ and layer (3) a measurable resistance of 60-400 kΩ. Given the greater resistance of layer (3) despite greater gas boron concentration, it could be inferred that the increased microwave power density reduced the uptake of boron or simply hindered the growth. Achard et al. showed that increasing microwave power density can decrease the doping efficiency during growth [28].

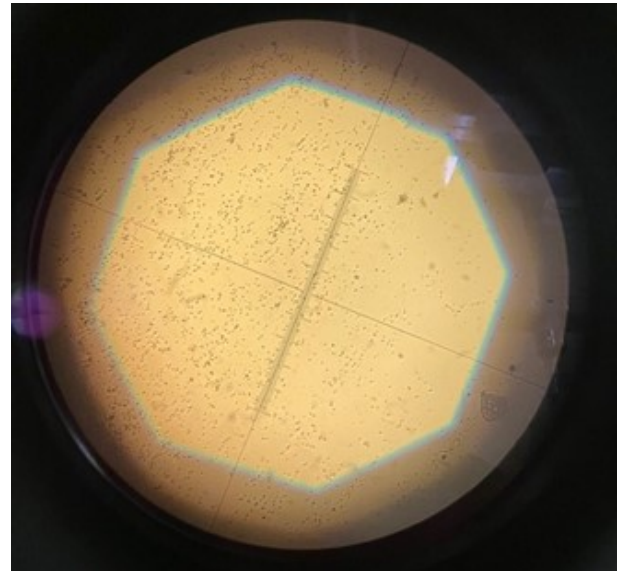


Figure 3.1: 50x optical image of layer (3)'s surface. The surface is frequently spotted, a sign of non-homoepitaxial growth

Both samples produced non-ohmic I-V curves measured using the Hall measurement kit with a clear bend around the 0 amp mark. For the diode construction, an ohmic contact is attached to this layer so these would be unacceptable for use in the diode structure, without even considering their very high resistances.

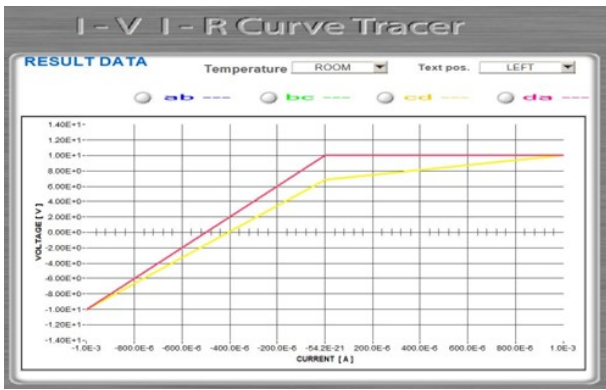


Figure 3.2: I-V curve produced by layer 3. The curve is non-ohmic as it lacks proportionality.

Attempts were made to take SEM images of the surfaces to visualise the bumps seen under the optical microscope however this proved a challenge due to the low conductivity of the samples and thus their tendency to charge during imaging. One image of layer (2)'s surface shows several black spots, around 1-5 μm s in diameter, possibly spots of undoped diamond that have grown through recrystallisation on the surface during the run. Visible on the samples is a bright frame running along the edges, possibly an area with greater boron uptake than the rest of the sample. This framing effect does seem to be present in all microwave grown boron doped layers.

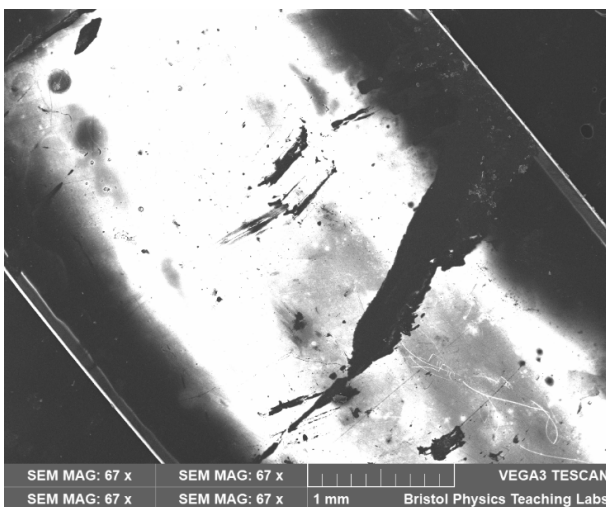


Figure 3.3: Zoomed out SEM image of layer 3. Around the edges, a bright frame is visible.

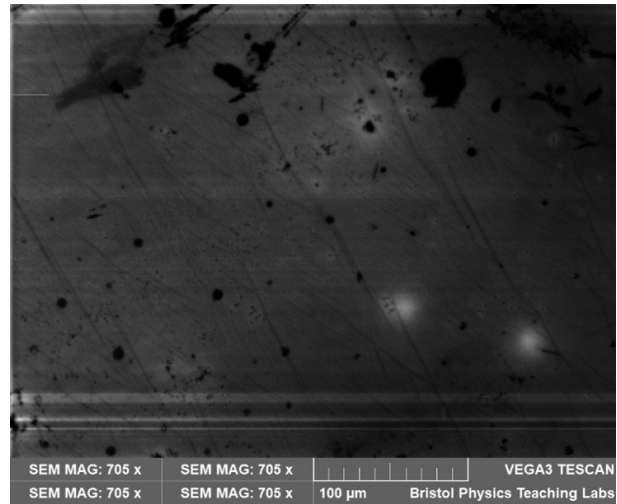


Figure 3.4: Zoomed in SEM image of layer 3. Notably, a number of black spots dot the surface, possibly the areas that form the bumps under the optical images.

Unfortunately, Raman spectra of the different samples were not very helpful. For all examined samples, a strong 1332 cm^{-1} peak was seen with no change in horizontal position or width, implying the spectra was only of the substrate and not the grown layer. This issue remained unresolved during the project.

3.0.4 Overview of Layer (4)

Layer (4) continues to look at the effect of temperature and forward power on the grown layers. This run lowered the temperature and pressure whilst keeping relatively high forward microwave power and increasing boron content. The hope was to improve upon layer 2 with 10 times the boron concentration in the gas mixture however results showed only a mild improvement with the sample only halving the resistance down to $30\text{k}\Omega$.

3.0.5 Analysis of layers (5) and (6)

(5) and (6) were grown using near identical conditions with the main difference being that (6) was grown the next day with a 4-hour growth run to try and improve upon the resistance measurements of (5). During the growth of (6) a second substrate was also present with a silicon mask covering a square section of the substrate. This was done to allow

for analysis of layer heights and to establish masking methods required when growing the intrinsic layer.

To probe the low microwave density region of parameter space further, forward power must be decreased. This, however, would lead to low substrate temperatures that would make growth infeasible. To remedy this, the spacer wire was swapped for one of near double thickness. This reduced the substrate holder's contact with the cooling stage, giving a higher equilibrium temperature. As temperature seemed to have little effect so far, a high temperature was targeted for these runs.

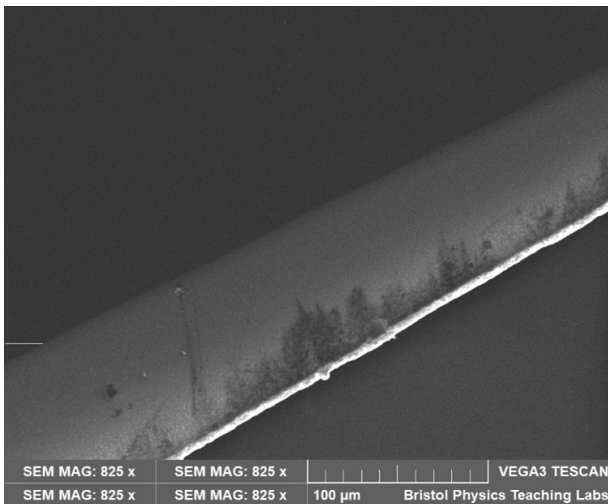


Figure 3.5: SEM image of layer (6), visible on this image is the conductive frame running around the edges of the sample

Immediately after retrieval from the reactor it was clear that the grown layers were different to before as they now took on a dark blue appearance. Measuring the two-probe resistance of layer (5) yielded a resistance of $3.91 \text{ k}\Omega$ and for the thicker layer (6) $1.7 \text{ k}\Omega$, a significant reduction in resistance.

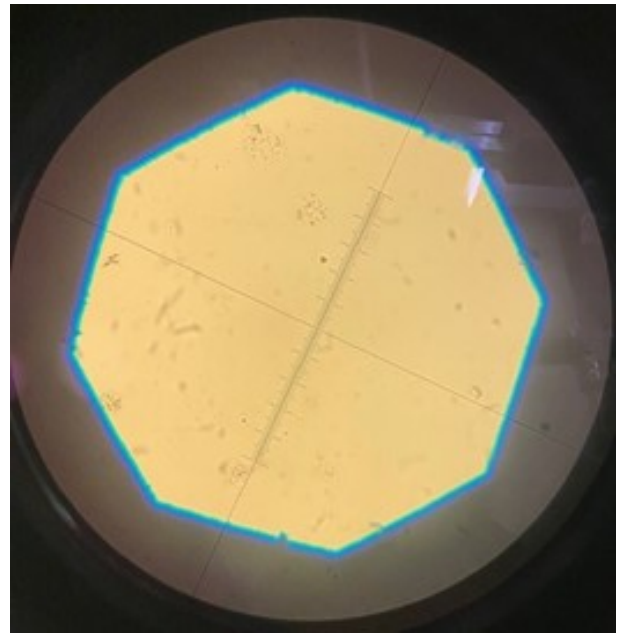


Figure 3.6: 50x optical image of layer (6)'s surface. Features only small clusters of spots and thus is a lot smoother.

Visible around the edges of layer (6) was a dark frame. It is expected that for closer probes, the resistance would be less as the current needs to flow through less resistive material. However, by moving the probe through this frame, larger probe distances gave smaller resistance values. This implies that this frame had much higher conductivity than the rest of the layer, and given its darker appearance, possibly a higher concentration of boron.

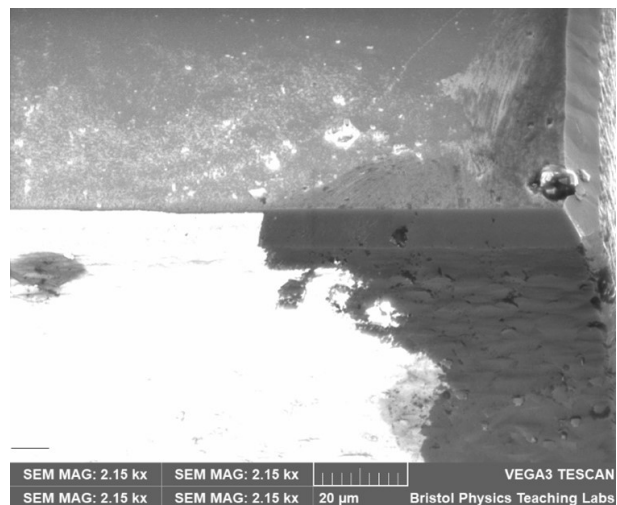


Figure 3.7: SEM image used to determine the height of layer (6), image of the masked sample. Image was taken at 45° off of the (110) surface.

Under the optical microscope, layer (6) had a significantly reduced number of bumps on its surface and these bumps were now localised into clusters. This was further shown in SEM images that present a very smooth surface. On the masked sample, SEM images show facets at 45 degrees to the (110) plane along the edges though only this sample shows them on one edge. Other edges and samples instead show overgrowth. The height of the facet from the masked layer (6) sample was measured with the plane of the camera parallel as $8.3 \mu\text{m}$ using the scale on the SEM. Assuming this as the hypotenuse for a 45-degree isosceles right triangle, this gives a layer height of $5.9 \mu\text{m}$ for the 4-hour growth or approximately $1.5 \mu\text{m h}^{-1}$.

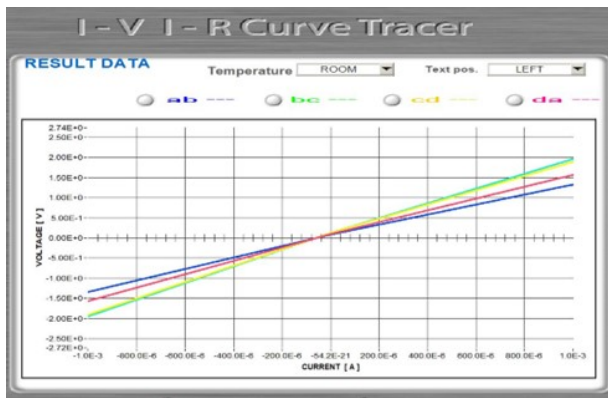


Figure 3.8: I-V curve of layer (6). Shows much more linear character than previously grown layers.

Hall measurements were also conducted on the unmasked layer (6) sample. Using the device's I-V mode, an ohmic curve was produced for each pair of corners. Using the layer height from above, Hall measurements were conducted on the unmasked layer (6) and important electrical characteristics tabulated in table 3.2. The readings are somewhat muddled as the sign of the sheet conductivity is flipped for the third row, implying n-type doping. This is extremely unlikely given the sole use of boron as a dopant and that the other readings all imply p-type. Definitive values for bulk carrier concentration are difficult to ascertain due to the variance in the data but are clearly of the magnitude of just over 10^{19} carriers cm^{-3} . This concentration is assumed to be roughly that of boron atoms in the layer, though is

most likely an underestimate. As a check, the resistivity here provides some agreement with the resistance measured on the two-probe device if the layer is assumed to have a resistance per unit length of the resistivity / (thickness * width) where the width is 0.3cm and the length 0.6cm. This lowest resistance scenario gives about 600Ω , around a third of the measured value.

3.0.6 Analysis of a hot filament grown layer

To provide a comparison to other CVD methods, a typical conductive boron doped layer was grown on the same kind of substrates by Mr Ramiz Zulkarnay on the hot filament reactor system. These layers are generally characterised by being thinner, usually 2-3 μm but are generally less resistive than similar samples grown on other systems.

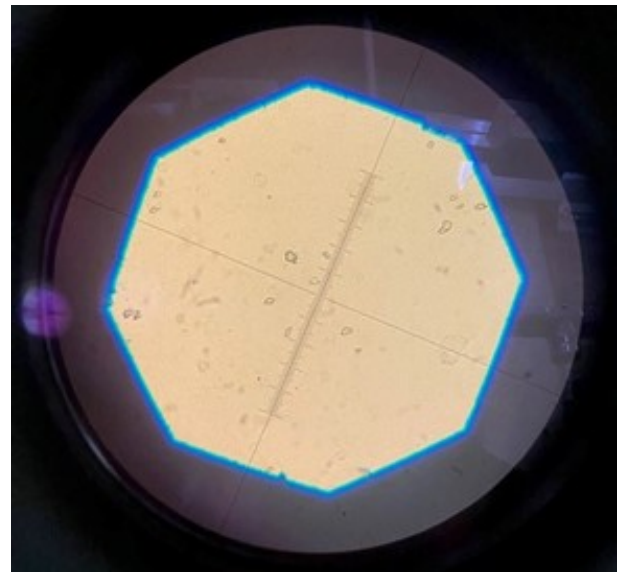


Figure 3.9: 50x optical image of the hot filament grown p-layer. Large spots can be seen on the surface, likely from pits.

With a two-point probe analysis of the layer, a resistance of 600Ω was measured, less than half of that measured for layer (6).

Under the optical microscope, the HF grown layer featured wide marks, possibly pits or nucleation sites, but otherwise was similarly smooth in appearance to layer (6). Notably, the sample sees a pattern on its surface of a dark

interior, a lighter section and a dark border. Compared to layer (6), the sample is much darker in this central region but approximately similar in tone for the light section. The sample also features a prominent scar that was not removable through the acetone wash method. SEM images of the sample were taken from presumably its underside, showing the polishing pattern left during production of the substrate. This image provides a good estimate for the layer height at approximately $2.6 \mu\text{m}$, similar to previous heights achieved on the HF system.

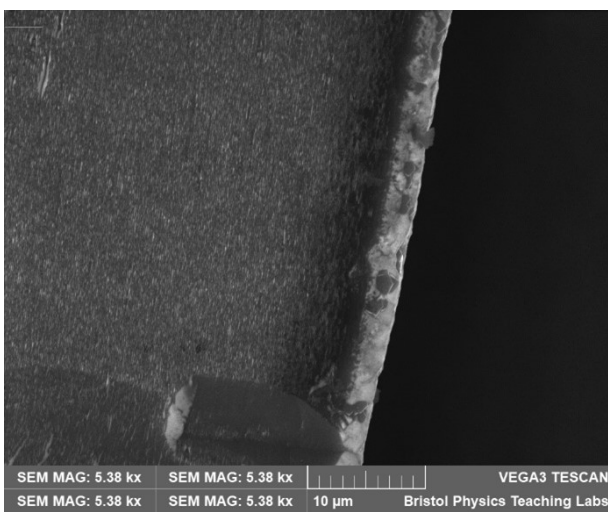


Figure 3.10: SEM image of the hot filament grown p-layer. Most likely the underside, the width of the light region is taken as a conservative estimate for the layer height.

The HF grown layer was also subjected to an I-V curve measurement on the Hall device, showing a similarly ohmic line to layer (6) but with a smaller gradient. Here the gradient is proportional to the resistance, confirming the two-point probe's lower resistance measurement. The HF sample featured a greater percentage difference in its minimum and maximum gradients going from 300Ω to 650Ω , a 117% increase, compared to a rise from 1250Ω to 2000Ω , a rise of 60%.

Using the layer height above and the hall measurement system, the bulk resistivity was found as approximately $7 \times 10^{-2} \Omega\text{cm}$ compared to layer (6)'s $1.8 \times 10^{-1} \Omega\text{cm}$, again less than half. This also means that the HF sample

has approximately double the conductivity of layer (6). During Hall measurements the sheet conductivity measurements would regularly be negative for small currents, tabulated in table 3.2 are the found values at a number of input currents. Notably, the values for sheet conductivity are approximately the same for both layers along with the Hall mobility. This is possibly due to the probe placement on the samples being on top of layer (6)'s frame and thus providing a more conductive pathway for that sample than the two-point measurement would have suggested. The bulk carrier concentrations of the two layers also appear broadly similar to each other.



Figure 3.11: Photo of the 3 samples grown: bottom left is the hot filament sample, top is layer (6) and bottom right is the masked layer (6) sample. Notice how much darker the hot filament sample is, implying a greater concentration of boron.

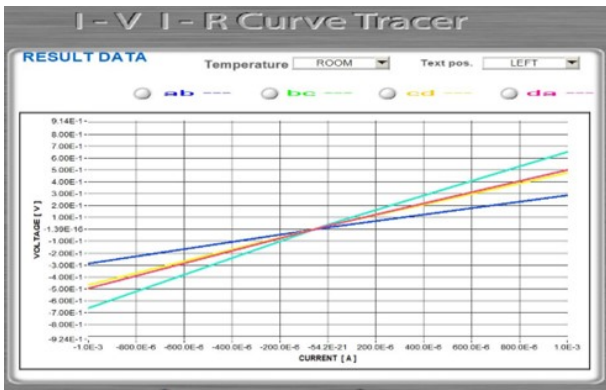


Figure 3.12: I-V curves of the hot filament grown p-layer.

I / A	Sheet Conc. / cm ⁻²	Bulk Conc. / cm ⁻³	Sheet Resistance / ohm	Bulk Resistivity / ohm cm	Hall mobility / cm ² V ⁻¹ s ⁻¹
5.00E-03	1.43E+16	2.43E+19	2.79E+02	1.64E-01	1.56E+00
1.00E-03	5.14E+16	8.72E+19	2.84E+02	1.67E-01	4.28E-01
5.00E-04	-1.72E+16	-2.92E+19	3.14E+02	1.85E-01	-1.16E+00
5.00E-04	1.51E+16	2.56E+19	3.13E+02	1.85E-01	1.32E+00
5.00E-04	-5.93E+16	-2.28E+20	1.04E-01	2.69E-05	-1.02E+03
2.00E-03	4.67E+16	1.79E+20	3.05E+02	7.92E-02	4.40E-01
2.00E-03	-1.01E+16	-3.88E+19	3.05E+02	7.92E-02	-2.04E+00
2.00E-03	5.63E+15	2.16E+19	3.05E+02	7.92E-02	3.65E+00
1.00E-03	1.04E+16	3.98E+19	2.71E+02	7.04E-02	2.23E+00

Table 3.2: Hall measurement data for layer (6) in white and the hot filament grown layer in grey. Both show similar bulk carrier concentrations but the HF layer has approximately half the bulk resistivity.

3.0.7 Growing the Intrinsic Layer

Now with appropriate boron doped layers, the intrinsic layer can be grown on top. This required a mask to allow for some exposed p-layer to remain for contact placement. Previously for layer (6) a small piece of silicon wafer was used as a mask however this introduced a couple problems. First is that manoeuvring a small piece of silicon over the required area is difficult without moving the underlying substrates out of the centre of the chamber. To remedy this, a molybdenum substrate holder had two spaces milled out of it to place the layer (6) and HF grown samples in together. Now the substrates wont shift during mask placement and the mask can lie flush with the layer-top of the holder plane. To mask the samples, a long, thin piece of silicon was placed onto one end of the samples covering around 1-2 mm. To ensure similar i-layers, both samples were grown on simultaneously.

How to grow an i-layer is not a straightforward process. The chamber is contaminated with boron so any samples will be lightly doped during growth. Additional gases such as oxygen and nitrogen can be used in the plasma to react away the boron but it's unknown how these would affect the growth of the layer itself. Given time constraints, it was decided to go ahead with a solely methane and hydrogen mix as there would not be enough time to produce more layers after the current samples had been metallised and examined.

Before growth the usual tungsten spacer wire had snapped so was replaced however, it was unclear if the new wire was of the same thickness. The pyrometer for the system had also become misaligned meaning that temperature measurements were not possible during the growth, compounding the new wire's problems.

For the growth, similar conditions were used as

normal with a power of 1.25 kW, pressure of 90 Torr and a methane content of 1% in the gas mixture. This layer was grown for 2 hours so was assumed to have a thickness of 3 μm .

3.0.8 Analysis of the intrinsic layer

Both grown intrinsic layers had similar end-to-end resistances measured on the 2-probe system of around 100 k Ω , though given that the layer lies on a much less resistive layer, this is not comparable to layers solely grown on the single crystal substrates.

Visually, the section covered in the I layer appeared darker with the microwave dark-frame visible on both samples. Using the optical microscope, both samples appeared like their respective under layers. A clear border can be seen between the masked and unmasked regions.

Samples were only imaged on the SEM after oxygen terminations and metallisation, so it's unclear which features are owed to which step. A clear border can again be seen in tone between the masked and unmasked regions but no physical step in height is present. A step would be unlikely given that the cleaved silicon wafer would not have provided a perfectly flat and flush surface for masking. The layer (6) sample appears to feature some pitting toward one edge though otherwise the grown layers are featureless, similar to layer (6)'s SEM images.

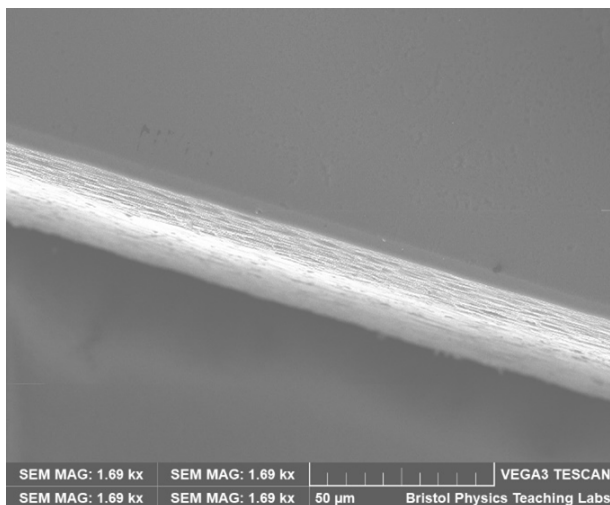


Figure 3.13: SEM image of the microwave grown sample's i-layer. Pitting appears present in the top right hand quadrant of the image.

3.0.9 Preparation for Metallisation

For proper adhesion to the diamond surface, the diamond must be oxygen terminated. As discussed in the section on oxygen terminations, a UV ozone cleaner was chosen for this role as it provides a gentler procedure. With 20 minutes of exposure, the surface is expected to possess a single monolayer of oxygen atoms coordinated randomly between the ketone and ether arrangements.

3.0.10 Metallisation

To provide the contacts for the diode, more masks are required. The ohmic contact is the easiest in this regard, it can just reuse a similar silicon wafer mask to that used in the growth of the i-layer, but instead leaving only the p-layer exposed. By loading thin nichrome wire into a boat filament for metal source 1 and gold rod into a coiled filament for metal source 2, the system was ready for metallisation. 10.2 nm of nichrome was deposited followed by 99.9 nm of gold. The nichrome wire used was Goodfellow 80:20 (nickel : chromium) wire however during evaporation, the stoichiometry of the metals may have changed. The gold rod was 99.999% purity from Alfa Aesar.

For the second contact, a small central contact was desired. If the contact were to go toward the edges, it may overlap with the dark frame on the samples, possibly shorting the diode. For this, a rectangular piece with a smaller rectangle cut out was used. Source 2 remained the same though source 1 was swapped with Goodfellow 99.5% purity aluminium wire. Unlike the previous mask, this deposition had shadowing effects owing to the edges of the mask blocking some of the sample from the metal source on either side. The nichrome layer was deposited to a thickness of 10.2nm and the gold layer to 99.2 nm.

Density of materials was taken as 19.32 g/cm for gold, 8.40 g/cm for the nichrome and 2.70 g/cm for the aluminium.

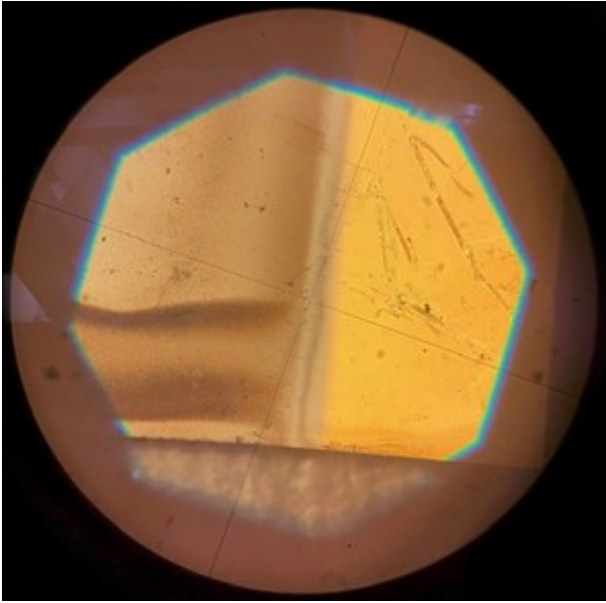


Figure 3.14: 10x zoom optical image of the hot filament grown diode's ohmic contact. Notice that the contact appears to lie wholly on the exposed p-layer as desired.

The final contacts were all satisfactorily placed: The ohmic contact ended before the colour change on the surface, confirmed with an optical microscope and the Schottky contact appeared to be placed centrally enough to avoid the dark frame on the i-layer.



Figure 3.15: Photo of the diodes diode immediately after metallisation. Above is the hot filament grown diode and below the microwave grown diode.

3.0.11 Characteristics of produced devices

Both devices were placed onto the 2 point-probe stage which had recently been modified to allow for I-V curves to be produced. The applied voltage range was set to -5.00×10^{-2} to 5.00×10^{-2} V to avoid saturating the multimeter. The program on the system then stepped in sizes of 1×10^{-3} V, taking 10 measurements for each applied voltage. All these points are then plotted to produce figure 3.16. For both devices, the current measured at each step was concordant for all 10 readings. Looking at the produced curves, it becomes

quickly obvious that they are not rectifying and are in fact near perfect straight-line graphs. They possess a squared R value of 1 implying no deviation or inflection that would be expected for diodes. The gradient of these lines is proportional to the conductivity and thus the reciprocal of the resistance for the devices. Strangely, the microwave grown device based on layer (6) has the lower resistance of 555.6Ω compared to the hot filament increased resistance of 3333.3Ω . Given the pseudo vertical structure, a different resistance to the original two probe measurements makes sense

but for one to increase and the other decrease points to some interesting being phenomena at play.

Both diodes were imaged using SEM and showed relatively featureless, flat surfaces with possibly some pitting on the top surface (as mentioned in the intrinsic layer section) maybe caused by the ozone treatment or created during growth of the i-layer. Visible on the contacts are scratch marks caused by the I-V measurement probes sharp ends. It appears on the ohmic contact of the microwave sample that this scratching has exposed a portion of the p-layer.

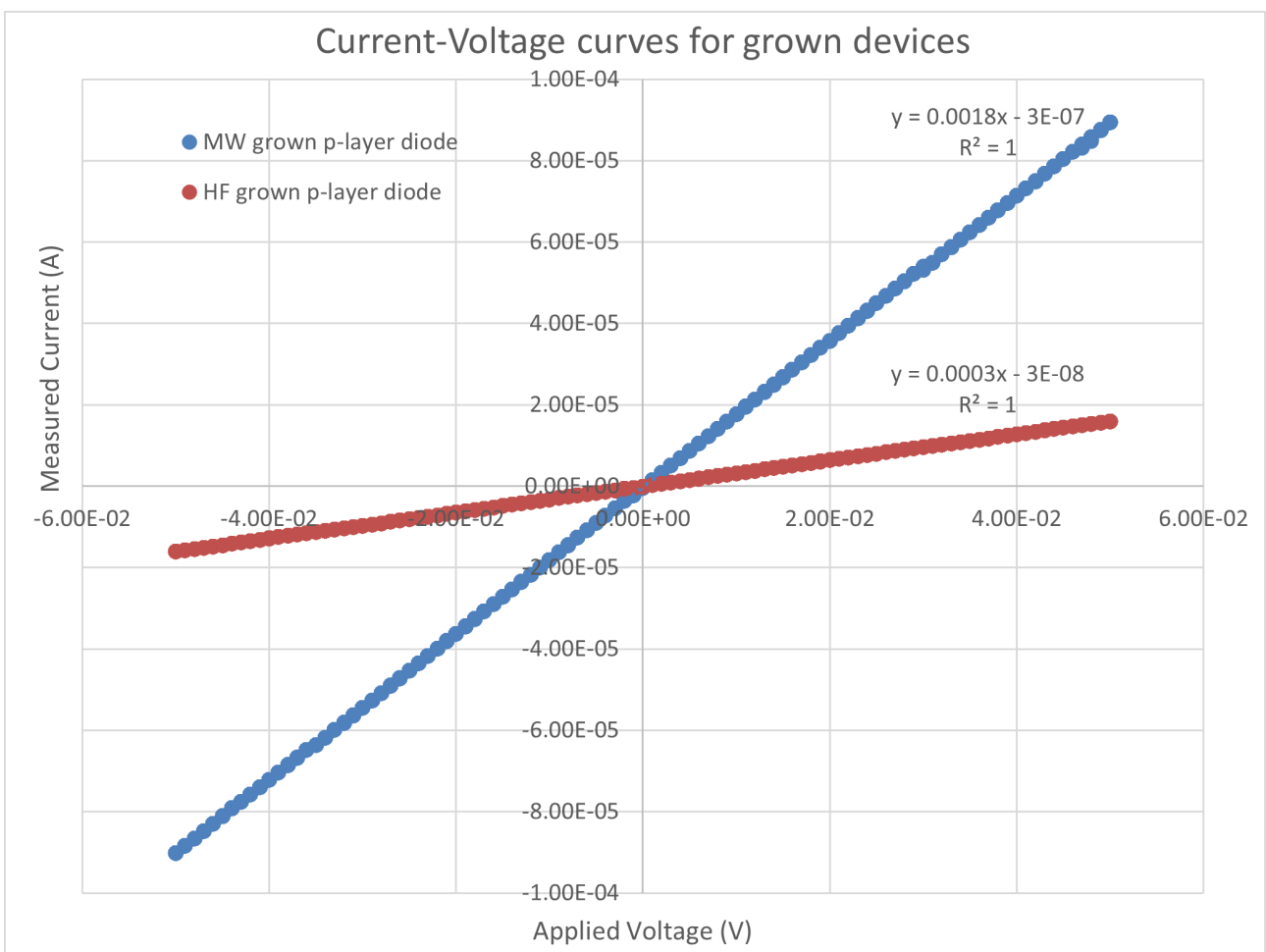


Figure 3.16: Resultant I-V curves of the two diodes. They show a completely linear relationship in this range, chosen as larger voltages saturated the ammeter.

Chapter 4

Discussion, Conclusion and Extensions

With the steps taken, a rectifying diode was expected. The following sections will examine the assumptions and problems with individual steps in the method, to attempt to explain the discrepancy in behaviour. Given that two different p-layers both gave the same ohmic result, the error is assumed to lie in the i-layer or with the contacts.

4.0.1 Different properties of oxygen terminated, (110) orientated diamond

As mentioned previously, different crystallographic orientations have different electron affinities and work functions, especially when functionalised, in this case with oxygen. No exact values are available precisely for these parameters on (110) so it was approximated that these matched with (100) diamond. Therefore, the Schottky barrier height for the aluminium contact was assumed to be about 1.16 eV [33]. It could be that the barrier height is smaller for (110) orientated diamond, lowering the rectification ratio and producing an ohmic shaped I-V curve or even that the difference between the metal work function and electron affinity is greater than the semiconductor band gap, eliminating the barrier.

4.0.2 Small depletion region width

For an ohmic I-V curve to be produced, one possibility is that the device must be operating with a depletion region width too small to maintain the built in potential of the junction, given the critical electric field strength of the

material. Diamond possesses a very large value of 7.7 to 20 MV cm⁻¹, so only a small i-layer was utilised in the design. Given the applied voltage was at most 50 mV, any depletion region width over 6.5x10⁻¹¹ m would operate without field breakdown. Of course, at this scale tunnelling would dominate [24]. The dopant concentration in the i-layer was not estimated, so direct calculation of the depletion region width is not possible. Assuming a worst-case scenario where the dielectric constant of the material (ϵ_s) is that of a vacuum (8.85x10⁻¹² Fm⁻¹), the dopant concentration (N_D) equal to the carrier concentration of the p-layer (3x10¹⁹ cm⁻³) and built in potential (ψ_{bi}) just the barrier height minus the acceptor level (1.16 - 0.37 eV), an estimate can be made by [24]:

$$w_D = \sqrt{\frac{2\epsilon_s}{qN_D}(\psi_{bi} - V - V_T)} \quad (4.1)$$

This value comes out as 3 nm, small enough to give this theory credit. Unintentional doping levels around 10¹⁵ to 10¹⁶ cm⁻³ would push the width to 400 nm, suitable for a diode. If the i-layer featured more dopants than expected, this could explain the ohmic nature of the I-V curves.

4.0.3 Poor contact at the junctions

Discontinuity at the Schottky contact interface can lead to a change in the Schottky barrier height. To match the Fermi levels of the metal and semiconductor, charge must be transferred based on the electronegativities of both materials. This transfer produces the dipole responsible for the Schottky barrier height. For small enough contact sizes, tunnelling rather than usual conduction, dominates through this barrier [47]. This can lead to fully ohmic appearing I-V curves for very small contact sizes. Given the pitting visible on the i-layer in the SEM images, it may be possible that the junction is discontinuous and thus is only contacting over small areas. The surface pits appear to be small and somewhat regularly spaced with maximum radii on the order of 1 μ m. Given the results of this work examining the effects of small contacts on Schottky devices [47], it seems that such dimensions

are too large in this case. One note is that the contacts were readily scraped away by the I-V curve probes, showing low adhesion to the diamond surface, perhaps indicative of a discontinuous surface.

4.0.4 Piercing of the Contacts by the Probes

With the probes being able to scrape away contact material, it's possible that the junction was formed between the p-layer/i-layer and the probe metal rather than the expected deposited contact metals. Multiple runs of I-V measurements were taken at differing probe angles, but they all yielded the same, most likely ruling out this possibility. Even with the gold probes, a Schottky barrier height of 0.98 eV [33] would be expected for the O-terminated boron doped diamond, which can be expected to influence the I-V curve.

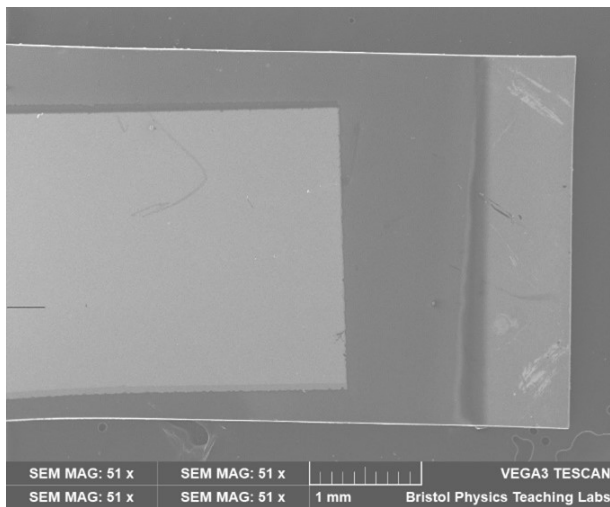


Figure 4.1: SEM plan image of the microwave grown diode. Notice the scratch marks present on the right ohmic contact from the I-V probes.

4.0.5 Tests and Treatments for Identified Problems

One possibility was that the assumption that the (110) diamond closely tracked the properties of the (100) diamond was incorrect. To account for this, further study of the (110) orientation is required such as determining its work function, electron affinity and its Schottky barrier with different contact metals. The first two can

be found through photoemission spectroscopy and inverse photoemission spectroscopy [23] though the latter requires a successful Schottky contact to determine.

A similar possibility is that the surface may not have been fully oxygen terminated by the UV ozone treatment. A technique such as x-ray photoelectron spectroscopy [23] can be utilised to find the elemental composition of adsorbates on the surface. It would also be useful to try alternate treatment times and techniques, such as O₂ plasma, to determine the different effects on the surface.

Another identified cause of failure was the possibility of an over doped i-layer. The first test could be to conduct hall measurements on an identically grown layer on an insulating substrate. This could ascertain the dopant concentration, allowing for comparison to the desirable range of 10^{15} - 10^{16} cm⁻³. This test may not produce useful results given the resistive nature of the i-layer so another technique such as secondary ion mass spectrometry can be used to determine this [48]. If the concentration of boron was higher than expected, oxygen and/or nitrogen additions could be explored to remove dopant atoms.

The contacts themselves could be edited. One possibility is applying a silver paint to the contacts and bonding some wires to the device. This has the benefit of removing the sharp probes though it only acts to confirm whether the scraping was affecting measurements. Another option is the use of identical diamond layers but this time depositing a smaller, central Schottky contact. Given that the frame of more conductive material lies around the edge on the grown i-layer, a smaller contact will reduce the effective dopant concentration at the interface, possibly improving the diode. Similarly, a different mask could be used when growing the i-layer to give a larger exposed region for the p-layer, ensuring the current flows through the device in the expected arrangement.

4.1 Conclusion

In this work, a method for reproducibly growing conductive boron doped diamond layers on (110) orientated single crystal

substrates was found using microwave plasma assisted chemical vapour deposition. This method was then used to grow the p-type layer in a Schottky diode for comparison to similar boron doped layers produced by hot filament chemical vapour deposition. On top of these two p-type layers, an unintentionally doped diamond intrinsic layer was grown using MWCVD over a mask and then the surface oxygen terminated using ozone UV treatment. The treated layers were then metallised: nichrome/gold for the ohmic contact on the exposed p-layer and aluminium/gold for the Schottky contact on the i-layer. The I-V characteristics for the device were tested, demonstrating an ohmic behaviour. Given the different p-layers yet similar results, it was assumed that the device's defect lied in its i-layer or metal contacts. It was reasoned that this could be caused by over doping of the i-layer, leading to a thin depletion region and thus little rectification, poor contact at the junctions due to surface defects such as pits or by incorrectly assuming similar work functions and electron affinities between the (110) diamond and the more typical (100) diamond.

4.2 Possible Extensions

The purpose of this work is to work towards betavoltaic devices that be grown with the radiation source implanted within the materials. Although possible using typical MWCVD, gases of particular radioactive isotopes run through the system would become contaminated at the exhaust, making gas recycling difficult. A system that can provide growth using static flow conditions would thus be preferred. Such techniques exist such as those described in [49], so a useful extension would be the adaptation of the experiment procedure to those kinds of systems.

As described in the section discussing treatment of problems during production, several analysis techniques could be applied at different stages to better provide a picture of development. Chief among these is secondary ion mass spectrometry, or SIMS, which can identify the boron concentration within the grown layers [48]. This would allow for comparison vs the bulk carrier concentration found using Hall measurements to more accurately determine dopant concentration. Doing so is necessary for exploring less doped layers such as the i-layer. Another useful technique to get functioning is Raman spectroscopy. Although tried, the system only seemed to focus on the substrate rather than the grown layer, providing identical peaks for each sample. With functional spectra, diamond quality in the grown layers can be better compared, such as in the FWHM of the diamond 1332 cm^{-1} peak or by the presence of graphitic peaks.

Due to its relative simplicity, a pseudo vertical structure was adopted for the diode device. A truly vertical structure with an ohmic contact/p-layer/i-layer/Schottky contact structure could provide an interesting comparison. This would require different substrates for growth or a method for producing free standing diamond films.

Finally, due to time constraints only one procedure for growing conductive boron doped layers was found. Specifically, 1% methane content was maintained throughout all runs and could be increased. Doing so may increase the growth rate, useful in reducing necessary growth times, reduce effects like pitting on the surface but may also reduce diamond quality. Likewise other additives such as oxygen and nitrogen should be explored to better understand the magnitude of their impact on boron concentration and layer quality in the device.

Bibliography

- [1] N Donato, N Rouger, J Pernot, G Longobardi, and F Udrea. Diamond power devices: state of the art, modelling, figures of merit and future perspective. *Journal of Physics D: Applied Physics*, 53(9):093001, dec 2019.
- [2] Hitoshi Umezawa, Shinya Ohmagari, Yoshiaki Mokuno, and Junichi H. Kaneko. Characterization of x-ray radiation hardness of diamond schottky barrier diode and metal-semiconductor field-effect transistor. In *2017 29th International Symposium on Power Semiconductor Devices and IC's (ISPSD)*, pages 379–382, 2017.
- [3] Chris J.H. Wort and Richard S. Balmer. Diamond as an electronic material. *Materials Today*, 11(1):22–28, 2008.
- [4] Yu. V. Pleskov. Electrochemistry of diamond: A review. *Russian Journal of Electrochemistry*, 38(12):1275–1291, Dec 2002.
- [5] Chunlin Zhou, Jinsong Zhang, Xu Wang, Yushu Yang, Pan Xu, Peixian Li, Lu Zhang, Zhiyuan Chen, Huanran Feng, and Weiwei Wu. Review—betavoltaic cell: The past, present, and future. *ECS Journal of Solid State Science and Technology*, 10(2):027005, feb 2021.
- [6] Daniel Araujo, Mariko Suzuki, Fernando Lloret, Gonzalo Alba, and Pilar Villar. Diamond for electronics: Materials, processing and devices. *Materials (Basel)*, 14(22), November 2021.
- [7] Y. Zou, P. W. May, S. M. C. Vieira, and N. A. Fox. Field emission from diamond-coated multiwalled carbon nanotube “teepee” structures. *Journal of Applied Physics*, 112(4):044903, 2012.
- [8] Paolo Calvani, Alessandro Bellucci, Marco Girolami, Stefano Orlando, Veronica Valentini, Riccardo Polini, and Daniele M. Trucchi. Black diamond for solar energy conversion. *Carbon*, 105:401–407, 2016.
- [9] George R. Fern, Peter R. Hobson, Alex Metcalfe, and David R. Smith. Performance of four cvd diamond radiation sensors at high temperature. *Nuclear Instruments and Methods in Physics Research Section A: Accelerators, Spectrometers, Detectors and Associated Equipment*, 958:162486, 2020. Proceedings of the Vienna Conference on Instrumentation 2019.
- [10] Mingyang Yang, Qilong Yuan, Jingyao Gao, Shengcheng Shu, Feiyue Chen, Huifang Sun, Kazuhito Nishimura, Shaolong Wang, Jian Yi, Cheng-Te Lin, and Nan Jiang. A diamond temperature sensor based on the energy level shift of Nitrogen-Vacancy color centers. *Nanomaterials (Basel)*, 9(11), November 2019.
- [11] Zoë Ayres and Julie Macpherson. Diamond: More than just a gemstone. *Catalyst: Secondary Science Review*, 27(2), 2016.
- [12] Sally Eaton-Magaña, James E. Shigley, and Christopher M. Breeding. Observations on hpht-grown synthetic diamonds: A review. *Gems & Gemology*, 53(3):262–284, 2017.

- [13] Scott S. Dossa, Ilya Ponomarev, Boris N. Feigelson, Marc Hainke, Christian Kranert, Jochen Friedrich, and Jeffrey J. Derby. Analysis of the high-pressure high-temperature (hpht) growth of single crystal diamond. *Journal of Crystal Growth*, 609:127150, 2023.
- [14] R C Burns, A I Chumakov, S H Connell, D Dube, H P Godfried, J O Hansen, J Härtwig, J Hoszowska, F Masiello, L Mkhonza, M Rebak, A Rommevaux, R Setshedi, and P Van Vaerenbergh. Hpht growth and x-ray characterization of high-quality type iia diamond. *Journal of Physics: Condensed Matter*, 21(36):364224, aug 2009.
- [15] Vladislav Zhdanov, Pavel Smirnov, Lukasz Andrzejewski, Julia Bondareva, and Stanislav Evlashin. Comparative analysis of labor input required to produce one carat at different methods of synthesis and mining of diamonds. *Heliyon*, 8(11):e11519, November 2022.
- [16] Michael Schwander and Knut Partes. A review of diamond synthesis by cvd processes. *Diamond and Related Materials*, 20(9):1287–1301, 2011.
- [17] M. N. R. Ashfold, P. W. May, C. A. Rego, and N. M. Everitt. Thin film diamond by chemical vapour deposition methods. *Chem. Soc. Rev.*, 23:21–30, 1994.
- [18] Guan-Ren Lai, E N Farabaugh, A Feldman, and L H Robins. Deposition of diamond films in a closed hot filament CVD system. *J Res Natl Inst Stand Technol*, 100(1):43–49, January 1995.
- [19] Yehia M Manawi, Ihsanullah, Ayman Samara, Tareq Al-Ansari, and Muataz A Atieh. A review of carbon nanomaterials’ synthesis via the chemical vapor deposition (CVD) method. *Materials (Basel)*, 11(5), May 2018.
- [20] J.A. Smith, K.N. Rosser, H. Yagi, M.I. Wallace, P.W. May, and M.N.R. Ashfold. Diamond deposition in a dc-arc jet cvd system: investigations of the effects of nitrogen addition. *Diamond and Related Materials*, 10(3):370–375, 2001. 11th European Conference on Diamond, Diamond-like Materials, Carbon Nanotubes, Nitrides and Silicon Carbide.
- [21] Naoto Ohtake and Masanori Yoshikawa. Diamond film preparation by arc discharge plasma jet chemical vapor deposition in the methane atmosphere. *Journal of The Electrochemical Society*, 137(2):717, feb 1990.
- [22] Michael Vollmer. Physics of the microwave oven. *Physics Education*, 39(1):74, jan 2004.
- [23] Harald Ibach and Hans Luth. *Solid-state physics : an introduction to principles of materials science*. Springer, Berlin, 4th extensively updated and enl. ed. edition, 2009.
- [24] S. M. Sze, Yiming Li, and Kwok K. Ng. *Physics of semiconductor devices*. John Wiley & Sons, Inc., Hoboken, NJ, fourth edition. edition, 2021.
- [25] Charles Kittel. *Introduction to solid state physics*. John Wiley & Sons, Inc, Hoboken, NJ, eighth edition edition, 2005.
- [26] F. Silva, X. Bonnin, J. Achard, O. Brinza, A. Michau, and A. Gicquel. Geometric modeling of homoepitaxial cvd diamond growth: I. the 100111110113 system. *Journal of Crystal Growth*, 310(1):187–203, 2008.
- [27] C. J. Chu, R. H. Hauge, J. L. Margrave, and M. P. D’Evelyn. Growth kinetics of (100), (110), and (111) homoepitaxial diamond films. *Applied Physics Letters*, 61(12):1393–1395, 1992.
- [28] J. Achard, F. Silva, R. Issaoui, O. Brinza, A. Tallaire, H. Schneider, K. Isoird, H. Ding, S. Koné, M.A. Pinault, F. Jomard, and A. Gicquel. Thick boron doped diamond single crystals for high power electronics. *Diamond and Related Materials*, 20(2):145–152, 2011.

- [29] P. Hazdra, A. Laposa, Z. Šobáň, A. Taylor, N. Lambert, V. Povolný, J. Kroutil, Z. Gedeonová, P. Hubík, and V. Mortet. Pseudo-vertical mo/au schottky diodes on 113 oriented boron doped homoepitaxial diamond layers. *Diamond and Related Materials*, 126:109088, 2022.
- [30] E. Gheeraert, N. Casanova, A. Tajani, A. Deneuve, E. Bustarret, J.A. Garrido, C.E. Nebel, and M. Stutzmann. n-type doping of diamond by sulfur and phosphorus. *Diamond and Related Materials*, 11(3):289–295, 2002. 12th European Conference on Diamond, Diamond- Like Materials, Carbon Nanotubes, Nitrides & Silicon Carbide.
- [31] Toshinobu Banjo, Masaaki Tsuchihashi, Minoru Hanazaki, Mutumi Tuda, and Kouichi Ono. Effects of o2 addition on bcl3/cl2 plasma chemistry for al etching. *Japanese Journal of Applied Physics*, 36(7S):4824, jul 1997.
- [32] J E Butler, M W Geis, K E Krohn, J Lawless Jr, S Deneault, T M Lyszczarz, D Flechtner, and R Wright. Exceptionally high voltage schottky diamond diodes and low boron doping. *Semiconductor Science and Technology*, 18(3):S67, feb 2003.
- [33] D. Doneddu, O.J. Guy, D. Twitchen, A. Tajani, M. Schwitters, and P. Igic. Schottky contacts on single-crystal cvd diamond. In *2006 25th International Conference on Microelectronics*, pages 179–182, 2006.
- [34] G.R. Mackenzie, S. Kaluvan, P.G. Martin, C. Hutson, T. Connolley, M. Cattelan, H. Dominguez-Andrade, T.L. Martin, N.A. Fox, and T.B. Scott. A diamond gammavoltaic cell utilizing surface conductivity and its response to different photon interaction mechanisms. *Materials Today Energy*, 21:100688, 2021.
- [35] Javier Navas, Daniel Araujo, José Carlos Piñero, Antonio Sánchez-Coronilla, Eduardo Blanco, Pilar Villar, Rodrigo Alcántara, Josep Montserrat, Matthieu Florentin, David Eon, and Julien Pernot. Oxygen termination of homoepitaxial diamond surface by ozone and chemical methods: An experimental and theoretical perspective. *Applied Surface Science*, 433:408–418, 2018.
- [36] J. van der Weide, Z. Zhang, P. K. Baumann, M. G. Wensell, J. Bernholc, and R. J. Nemanich. Negative-electron-affinity effects on the diamond (100) surface. *Phys. Rev. B*, 50:5803–5806, Aug 1994.
- [37] Gary Wan, Mattia Cattelan, and Neil A. Fox. Electronic structure tunability of diamonds by surface functionalization. *The Journal of Physical Chemistry C*, 123(7):4168–4177, Feb 2019.
- [38] Vadim Lebedev, Jan Engels, Jan Kustermann, Jürgen Weippert, Volker Cimalla, Lutz Kirste, Christian Giese, Patricia Quellmalz, Andreas Graff, Frank Meyer, Markus Höfer, and Volker Sittinger. Growth defects in heteroepitaxial diamond. *Journal of Applied Physics*, 129(16):165301, 2021.
- [39] Steven Praver and Robert J. Nemanich. Raman spectroscopy of diamond and doped diamond. *Philosophical Transactions of the Royal Society of London. Series A: Mathematical, Physical and Engineering Sciences*, 362(1824):2537–2565, 2004.
- [40] Gurvinder Singh Bumrah and Rakesh Mohan Sharma. Raman spectroscopy – basic principle, instrumentation and selected applications for the characterization of drugs of abuse. *Egyptian Journal of Forensic Sciences*, 6(3):209–215, 2016.
- [41] V. Mortet, Z. Vlčková Živcová, A. Taylor, O. Frank, P. Hubík, D. Trémouilles, F. Jomard, J. Barjon, and L. Kavan. Insight into boron-doped diamond raman spectra characteristic features. *Carbon*, 115:279–284, 2017.

- [42] Krishanu Biswas, Sri Sivakumar, and Nilesh Gurao. *Electron microscopy in science and engineering*, volume 6. Springer, Singapore, 2022.
- [43] Kalsoom Akhtar, Shahid Ali Khan, Sher Bahadar Khan, and Abdullah M. Asiri. *Scanning Electron Microscopy: Principle and Applications in Nanomaterials Characterization*, pages 113–145. Springer International Publishing, Cham, 2018.
- [44] L. J. van der PAUW. *A METHOD OF MEASURING SPECIFIC RESISTIVITY AND HALL EFFECT OF DISCS OF ARBITRARY SHAPE*, pages 174–182. 1958.
- [45] E. H. Hall. On a new action of the magnet on electric currents. *American Journal of Mathematics*, 2(3):287–292, 1879.
- [46] W. Shockley. The theory of p-n junctions in semiconductors and p-n junction transistors. *The Bell System Technical Journal*, 28(3):435–489, 1949.
- [47] R. A. Kraya and L. Y. Kraya. The role of contact size on the formation of schottky barriers and ohmic contacts at nanoscale metal-semiconductor interfaces. *Journal of Applied Physics*, 111(6):064302, 2012.
- [48] A. L. Vikharev, A. M. Gorbachev, M. A. Lobaev, A. B. Muchnikov, D. B. Radishev, V. A. Isaev, V. V. Chernov, S. A. Bogdanov, M. N. Drozdov, and J. E. Butler. Novel microwave plasma-assisted cvd reactor for diamond delta doping. *physica status solidi (RRL) – Rapid Research Letters*, 10(4):324–327, 2016.
- [49] A. Croot, E.J.D. Mahoney, H. Dominguez-Andrade, M.N.R. Ashfold, and N.A. Fox. Diamond chemical vapor deposition using a zero-total gas flow environment. *Diamond and Related Materials*, 109:108011, 2020.